



Title	Foxo3-mediated physiological cell competition ensures robust tissue patterning throughout vertebrate development
Author(s)	Matsumoto, Kanako; Akieda, Yuki; Haraoka, Yukinari et al.
Citation	Nature Communications. 2024, 15, p. 10662
Version Type	VoR
URL	https://hdl.handle.net/11094/100425
rights	This article is licensed under a Creative Commons Attribution-NonCommercial-NoDerivatives 4.0 International License.
Note	

The University of Osaka Institutional Knowledge Archive : OUKA

<https://ir.library.osaka-u.ac.jp/>


The University of Osaka






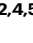

Foxo3-mediated physiological cell competition ensures robust tissue patterning throughout vertebrate development

Received: 31 October 2023

Accepted: 27 November 2024

Published online: 17 December 2024

 Check for updates

Kanako Matsumoto ^{1,2,6}, Yuki Akieda ^{1,6}, Yukinari Haraoka ¹, Naoki Hirono ³, Hiroshi Sasaki ³ & Tohru Ishitani ^{1,2,4,5} 

Unfit cells with defective signalling or gene expression are eliminated through competition with neighbouring cells. However, physiological roles and mechanisms of cell competition in vertebrates remain unclear. In addition, universal mechanisms regulating diverse cell competition are unknown. Using zebrafish imaging, we reveal that cell competition ensures robust patterning of the spinal cord and muscle through elimination of cells with unfit sonic hedgehog activity, driven by cadherin-mediated communication between unfit and neighbouring fit cells and subsequent activation of the Smad-Foxo3-reactive oxygen species axis. We identify Foxo3 as a common marker of loser cells in various types of cell competition in zebrafish and mice. Foxo3-mediated physiological cell competition is required for eliminating various naturally generated unfit cells and for the consequent precise patterning during zebrafish embryogenesis and organogenesis. Given the implication of Foxo3 downregulation in age-related diseases, cell competition may be a defence system to prevent abnormalities throughout development and adult homeostasis.

Animal development is highly reproducible and repeatedly generates tissues and organs with the same function. An appropriate number of cells with specific functions must be located at the correct positions to construct functional tissues and organs. Such spatial cell arrangements are regulated by genetic information and the corresponding biochemical signals^{1,2}. However, dynamic morphogenesis, including active rapid cell proliferation and migration during development, may induce replication errors and cellular signalling perturbations, generating unfit cells in developing tissues. Recent advances in single-cell analyses have revealed frequent generation of cells with somatic mutations or

chromosome segregation errors during normal human and mouse embryogenesis^{3–6}. Our zebrafish imaging analysis also showed frequent occurrence of unfit cells with abnormal Wnt/ β -catenin activity in normal embryos⁷. Considering the fact that developing animals achieve reproducible construction of functional tissues and organs, they must possess systems to overcome the generation of such unfit cells. However, the mechanisms underlying robust tissue development are not completely understood.

Cell competition may support conquering unfit cell appearance during early embryogenesis. Cell competition is a cell–cell interactive

¹Department of Homeostatic Regulation, Research Institute for Microbial Diseases, Osaka University, Suita, Osaka, Japan. ²Department of Biological Sciences, Graduate School of Science, Osaka University, Suita, Osaka, Japan. ³Laboratory for Embryogenesis, Graduate School of Frontier Biosciences, Osaka University, Suita, Osaka, Japan. ⁴Center for Infectious Disease Education and Research (CiDER), Osaka University, Suita, Osaka, Japan. ⁵Japan Agency for Medical Research and Development - Core Research for Evolutional Science and Technology (AMED-CREST), Osaka University, Osaka, Japan. ⁶These authors contributed equally: Kanako Matsumoto, Yuki Akieda. ✉ e-mail: ishitani@biken.osaka-u.ac.jp

process for removing less fit viable cells, which was discovered in *Drosophila*^{8,9}. Unfit cells with relatively low Myc expression, Yap activity, or mitochondrial defects spontaneously arise during early mouse embryogenesis; however, these cells are eliminated through competitive communication with neighbouring normal cells^{10–12}. Furthermore, cell competition corrects the noisy Wnt/ β -catenin morphogen gradient, which patterns the zebrafish embryonic anterior–posterior axis, by eliminating cells with abnormally high or low Wnt/ β -catenin⁷. Notably, inhibition of cell competition induces the accumulation of Wnt-unfit cells, thereby disturbing embryonic patterning⁷. Therefore, cell competition-mediated elimination of unfit cells ensures robust early embryogenesis. However, the roles and mechanisms of cell competition during later developmental stages, such as organogenesis, remain unclear.

Various factors, such as cells with abnormal Myc, Yap, Wnt/ β -catenin, and Ras activity, drive cell competition and mutations in ribosomal protein genes (collectively termed ‘Minute’) promote competitive interactions with neighbouring normal cells^{7,8,10–15}. Because different abnormalities can stimulate distinct signalling and gene expression pathways, unfit cells with different anomalies are eliminated through distinct mechanisms. Recent studies on *Drosophila* have revealed shared mechanisms of cell competition. For example, activation of Flower-Azot signalling^{16,17}, Toll receptor signalling^{18,19}, and autophagy²⁰ is commonly involved in Myc- and Minute-induced cell competition. However, these mechanisms do not always function in other competition contexts^{17,21}. Thus, the universal machinery regulating diverse cell competition types remains unknown. Moreover, most studies on cell competition have been conducted using genetic models that rely on the overexpression or mutation of specific genes. Consequently, the understanding of ‘physiological cell competition’, especially in vertebrates, remains elusive.

In this study, we explored the role of physiological cell competition and the universal machinery involved in vertebrate development using zebrafish imaging. We discovered cell competition-mediated correction of sonic hedgehog (Shh) morphogen gradients as previously unidentified roles of physiological cell competition during organogenesis and deciphered that Cadherin-Smad-Foxo3-reactive oxygen species (ROS) signalling mediates this cell competition. Moreover, we identified Foxo3 as an evolutionally conserved universal marker of unfit cells eliminated by various vertebrate cell competitions driven by Wnt, Shh, Ras, Myc, Yap, and ribosomal proteins. By analysing Foxo3 expression and function, we found that physiological cell competition-mediated elimination of endogenous unfit cells is essential in precise embryogenesis and organogenesis in vertebrates.

Results

Apoptosis supports precise neural and muscle patterning

We examined the effects of apoptosis inhibition on the spinal cord and muscle development in zebrafish to elucidate the role of cell competition-mediated apoptotic elimination of unfit cells during organogenesis. In the vertebrate spinal cord, various neural progenitor cells (e.g. p0, pMN, and floor plate), distinguished by specific transcription factors (*dbx1b*, *olig2*, and *foxa2*, respectively)^{22–26}, form stripe-like patterns along the dorso-ventral (DV) axis (Fig. 1a, b). In zebrafish muscle primordia, slow muscle precursors are at the periphery of the somites, whereas fast muscle precursors are located on the medial side²⁷. Muscle pioneer cells are adjacent to the notochord²⁸ (Fig. 1c, Supplementary Fig. 1a). Inhibiting apoptosis by overexpressing *bcl2a* mRNA, which encodes an anti-apoptotic protein, induced ectopic expression of the intermediate neural marker *dbx1b* and the ventral neural markers *olig2* and *foxa2* in the ventral and dorsal areas, respectively (Fig. 1b). Abnormal reduction in the expression of these markers was also observed (Fig. 1b). In the muscle primordium, the precise induction of fast and slow muscle fibres and muscle pioneer cells was disturbed, and some of these were mislocated (Fig. 1d–f).

Consistent with this abnormal neural and muscle patterning, some apoptosis-inhibited larvae exhibited abnormal morphogenesis (Supplementary Fig. 1b), and even morphologically normal larvae showed poor locomotion (Supplementary Fig. 1c). We also generated a transgenic zebrafish line carrying HS:GFP-zBcl2a, which inhibited apoptosis in a heat shock-dependent manner (Supplementary Fig. 1d) to examine the role of apoptotic elimination during organogenesis. Blocking apoptosis during organogenesis also induced distortion in organ patterning (Supplementary Fig. 1e, f), suggesting that apoptosis is required for precise spinal cord and muscle patterning.

Shh-unfit cells undergo apoptotic elimination

Shh morphogen signalling forms an activity gradient along the DV axis and specifies the distinct fate of each cell in a signalling activity-dependent manner in the developing spinal cord and muscle primordia (Fig. 2a)^{28–31}. Therefore, we hypothesised that apoptosis eliminates abnormal cells with unfit Shh-activity during neural and muscle development. To test this hypothesis, we visualised Shh signalling in the Tg(8xGBS:d2EGFP) zebrafish line, which expresses destabilised enhanced green fluorescent protein (d2EGFP) upon activating the Gli transcription factor family downstream of Shh signalling³² (Fig. 2b). Unfit cells with abnormally high or low Shh signalling activity appeared spontaneously in the Shh activity-low (dorsal) or Shh activity-high (ventral) regions of the spinal cord and muscle primordia, respectively (Fig. 2c, d). The number of unfit cells varied between larvae (left graphs in Fig. 2e, f), suggesting that the appearance of these cells is not part of the developmental programme but is the result of an error in the programme. In addition, 38% of unfit cells ($n = 11/29$) in the spinal cord and 31% of unfit cells ($n = 10/32$) in the muscle were active caspase-3-positive (Fig. 2c, d), suggesting that they undergo apoptosis. Moreover, apoptosis inhibition through *bcl2a* overexpression blocked the elimination of Shh-unfit cells and enhanced their accumulation (Fig. 2c–f). These data indicate that the apoptotic elimination of Shh-unfit cells is necessary for robust Shh morphogen gradient formation and precise neural and muscle patterning.

Substantial difference in Shh-activity triggers apoptosis

We artificially introduced Shh-unfit cells expressing fluorescent proteins (e.g. mKO2 or GFP) into the zebrafish spinal cord and muscle primordia by injecting heat-shock-driven expression plasmids to confirm that developing organs possess a system for eliminating cells with unfit Shh activity through apoptosis. A low-dose injection of the plasmids induced a mosaic distribution of fluorescent cells surrounded by normal cells (Fig. 3a). Shh-hyperactivated cells expressing constitutively active mutants of the Shh receptor Smoothed (SmoCA) and Shh-inactivated cells expressing the Shh negative regulator Ptch1 activated caspase-3, which gradually disappeared via DNA fragmentation. In contrast, cells expressing only mKO2 survived (Fig. 3b, c; Supplementary Fig. 2a–c, Supplementary Movie 1, 2). Bcl2a co-expression prevented the elimination of SmoCA-expressing cells (Supplementary Fig. 2a, b). Thus, developing organs can eliminate spontaneously appeared and artificially introduced Shh-defective cells. Furthermore, mosaically introduced SmoCA-expressing (Shh-high) cells or Ptch1-overexpressing (Shh-low) cells efficiently activated caspase-3 in the Shh signalling-low dorsal and signalling-high ventral regions, respectively (Fig. 3d, e). These results suggest that a substantial difference in Shh activity between unfit and neighbouring normal cells triggers apoptosis. Forced activation of Shh signalling through *SmoCA* expression or forced inactivation of Shh signalling via treatment with the Shh signalling inhibitor cyclopamine³³ in whole tissues (Supplementary Fig. 2d, e) hindered the elimination of Shh-high and Shh-low cells, respectively (Supplementary Fig. 2f, g). These results indicate that a large difference in Shh signalling activity between unfit cells and neighbouring fit cells is essential to trigger the apoptosis of unfit cells. Intriguingly, when SmoCA-expressing (Shh-

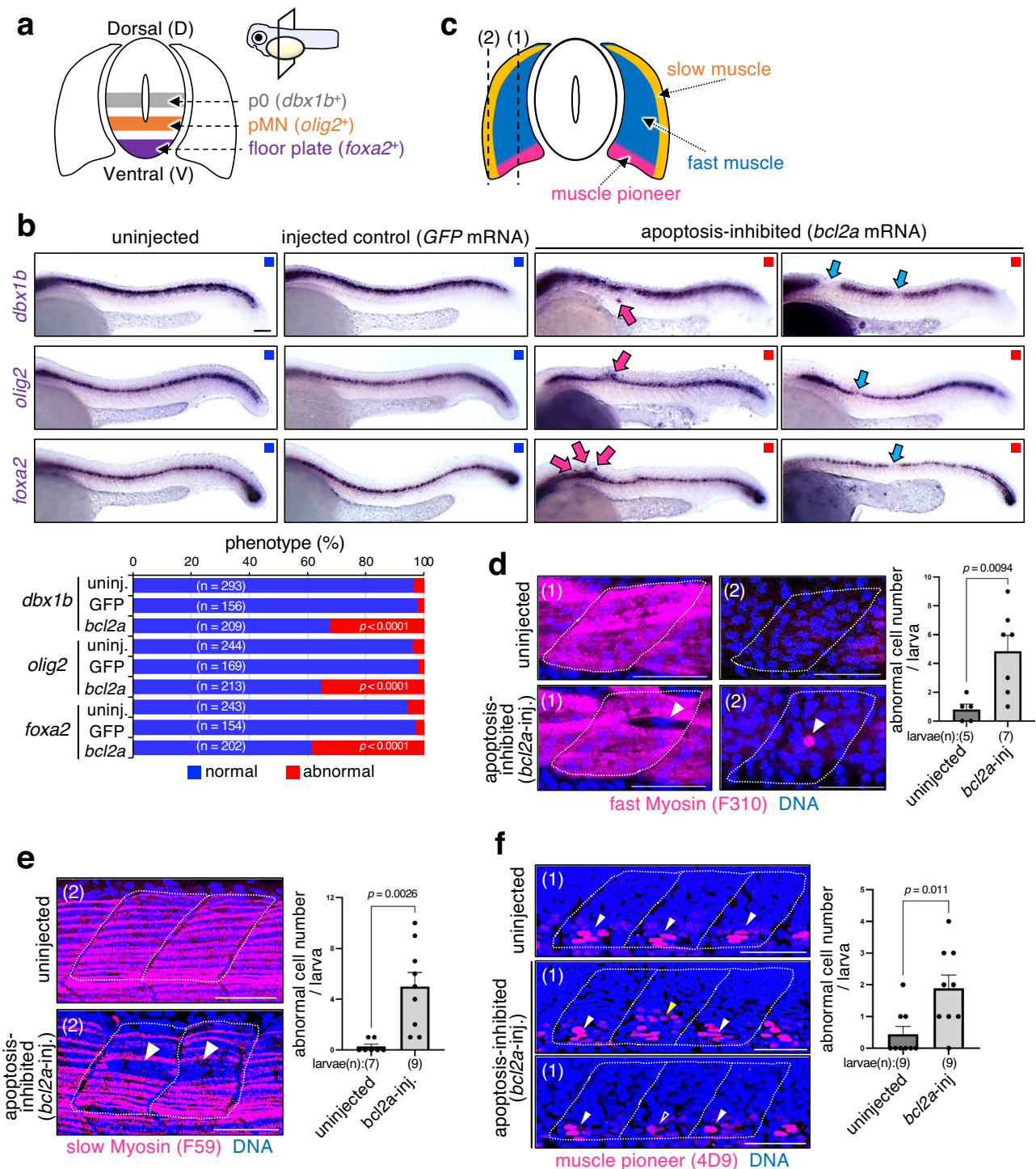


Fig. 1 | Apoptosis is essential for precise spinal cord and muscle patterning. **a** Schematic illustration of the expression patterns of *dbx1b* (a p0 neural progenitor marker), *olig2* (a pMN neural progenitor marker), and *foxa2* (a floor plate progenitor marker) in the spinal cord. **b** Inhibiting apoptosis distorts dorso-ventral (DV) patterning in the spinal cord. The panels show whole-mount in situ hybridisation of *dbx1b*, *olig2*, and *foxa2* in wild-type (uninjected), injected control (*GFP* mRNA-injected) and apoptosis-inhibited (*bcl2a* mRNA-injected) 24 h post-fertilisation (hpf) larvae. In abnormal larvae, *dbx1b*, *olig2*, and *foxa2* were ectopically activated or inactivated in discontinuous regions. The bottom graph shows the percentages of larvae with normal or abnormal expression patterns in uninjected, *GFP* mRNA- or *bcl2a* mRNA-injected (apoptosis-inhibited) larvae. Scale bar = 100 μ m. The chi-square test was used for statistical analysis. **c** Schematic

illustration of muscle cell pattern. The labels (1) and (2) in (d–f) correspond to the images of sections indicated as (1) and (2) in (c). **d–f** Apoptosis inhibition distorts gene expression patterns in the muscle primordia. The panels show whole-mount immunostaining for fast myosin (F310, fast muscle cells) (d), slow myosin (F59, slow muscle cells) (e), and muscle pioneer (4D9, muscle pioneer cells) (f), respectively (magenta). In abnormal larvae, fast myosin, slow myosin, and muscle pioneer proteins are ectopically expressed or are absent. Scale bar = 100 μ m. Bar plots on the right show the mean + SEM of abnormal gene expressing-cell numbers in wild-type (uninjected) and apoptosis-inhibited (*bcl2a* mRNA-injected) larvae. An unpaired two-tailed *t*-test was used for the statistical analysis. Source data are provided as a Source Data file.

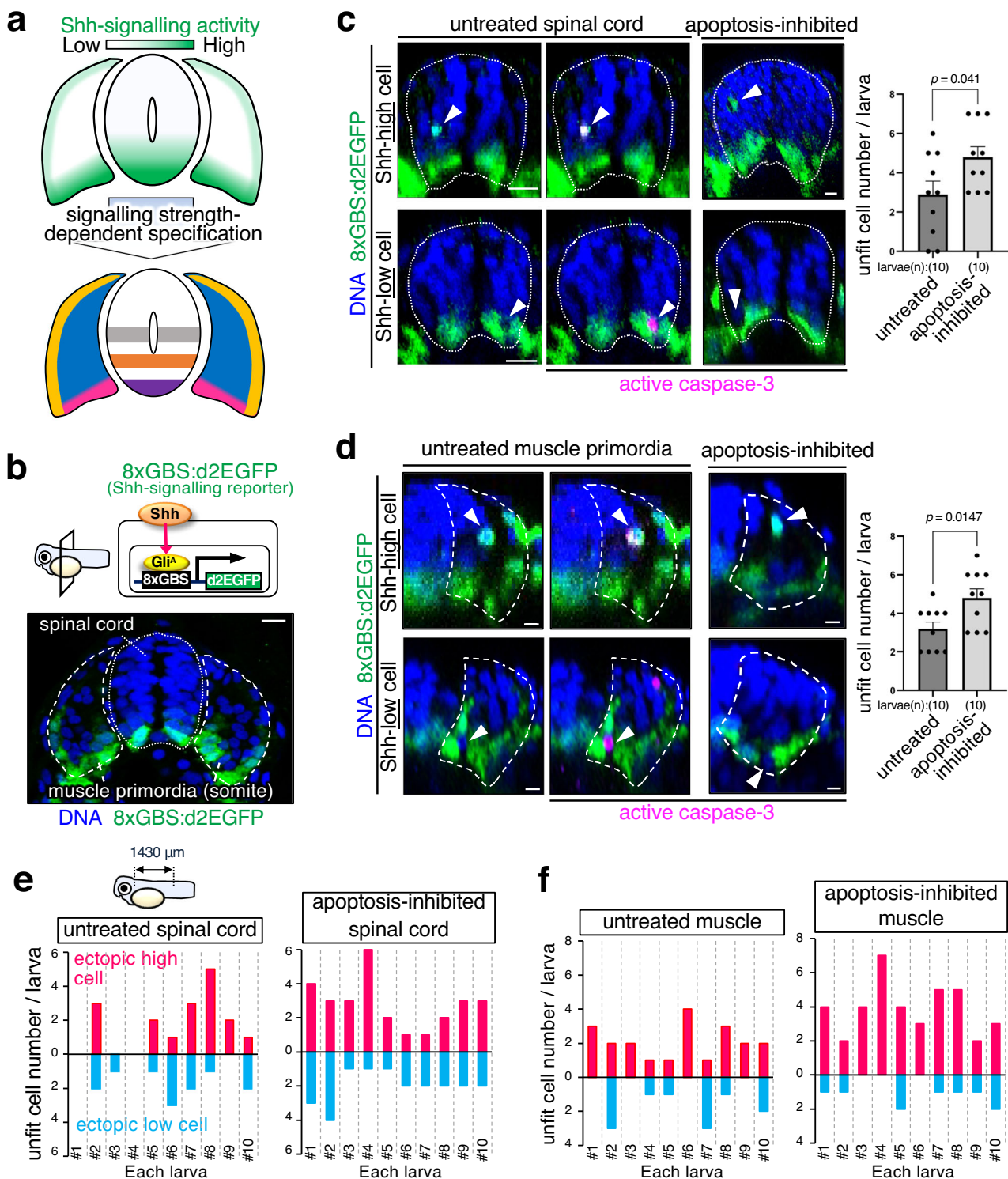


Fig. 2 | Shh-unfit cells are apoptotically eliminated. **a** The strength of Shh signalling activity mediates distinct cell types specification in the spinal cord and muscle. **b** In a horizontal plane, 8xGBS:d2EGFP drives destabilised enhanced green fluorescent protein (d2EGFP) expression in response to Shh signalling activation in the developing spinal cord and muscle of reporter larvae (cross-sectional view with the dorsal on top, 24 hpf). The dotted line and dashed line represent the spinal cord and muscle primordia boundaries, respectively. Scale bar = 10 μ m. **c, d** Caspase-3 activation in cells with impaired Shh signalling activity during spinal cord (**c**) and muscle development (**d**). Whole-mount immunostaining of d2EGFP (green) horizontal plane and active caspase-3 (magenta) in Tg(8xGBS:d2EGFP) zebrafish larvae

untreated or apoptosis-inhibited (*bcl2a* mRNA-injected). Arrowheads indicate cells with abnormal Shh signalling-reporter activity. Scale bar = 10 μ m. The bar plots show the mean + SEM of unfit cell frequencies in untreated and apoptosis-inhibited larvae. An unpaired two-tailed *t*-test was used for the statistical analysis. **e, f** Inhibiting apoptosis enhances the Shh-unfit cell accumulation in the spinal cord (**e**) and muscle (**f**). The bar plots show unfit cell frequencies in untreated and apoptosis-inhibited larvae. Each larva has a different number of spontaneously appearing unfit cells with abnormally high or low Shh signalling activity. Source data are provided as a Source Data file.

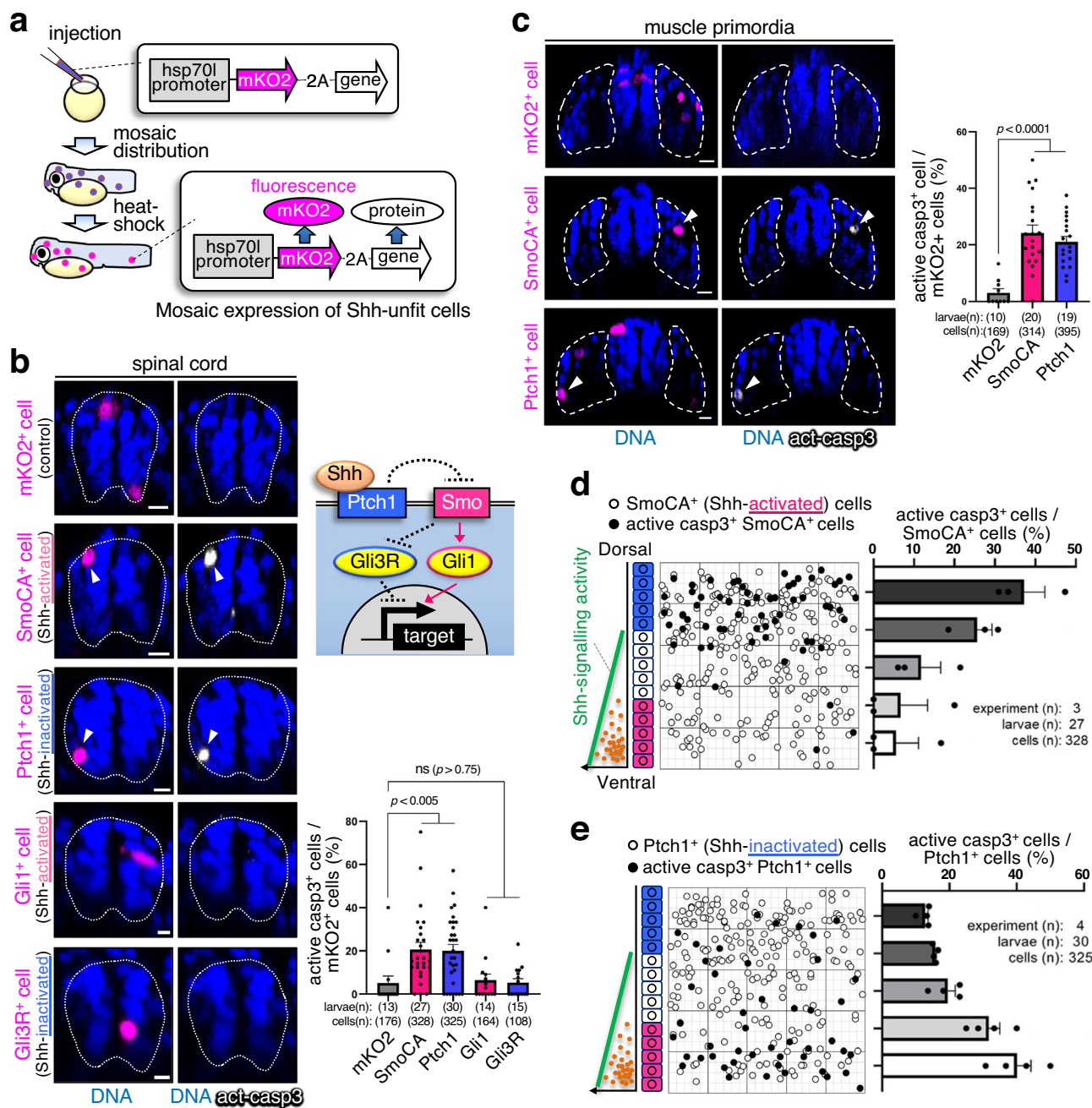


Fig. 3 | Substantial differences in Shh-activity trigger apoptosis. **a** Schematic diagram of the experimental introduction of abnormal fluorescent Shh signalling cells into zebrafish larvae in a mosaic manner through heat shock induction. **b, c** Artificially introduced SmoCA-expressing (Shh-activated) or Ptch1-overexpressing (Shh-inactivated) cells underwent apoptosis, but Gli1- or Gli3R-expressing cells did not undergo apoptosis in the spinal cord (**b**) and muscle (**c**). Confocal microscopy images show whole-mount immunostaining of active caspase-3 (grey) in mosaic larvae expressing mKO2 alone or with SmoCA, Ptch1, Gli1, or Gli3R (magenta). Arrowheads indicate caspase-3 active cells. Scale bar = 10 μ m. Bar plots show the mean \pm SEM of the mKO2⁺ and caspase-3-active cell frequencies. Two-tailed one-way ANOVA was used for the statistical analysis. **d, e** Cells causing substantial noise in the Shh gradient efficiently underwent apoptosis. The left panels show maps of artificially introduced SmoCA- or Ptch1-expressing cells in the zebrafish spinal cord. The graphs on the right show the mean \pm SEM of mKO2⁺ and caspase-3-active cell frequencies within a divided range along the dorso-ventral (DV) axis. Source data are provided as a Source Data file.

high) cells were clonally induced on the dorsal side of the spinal cord, those at the edge of the clone, surrounded by normal cells, underwent apoptosis efficiently (Supplementary Fig. 2h, i). However, the apoptosis efficiency in these cells decreased as the proportion of SmoCA cells in the surrounding adjacent cell population increased, and SmoCA cells inside the clone did not die (Supplementary Fig. 2h, i). These results indicate that merely being adjacent to cells with different Shh signalling activity is not enough to induce apoptosis of unfit cells but being surrounded by cells with different signalling activity (being a

minority in the population) is necessary for the induction of death in unfit cells. Notably, mosaic introduction of cells overexpressing the transcription factor Gli1 or the dominant negative form of the Gli3 transcription factor (Gli3R), which positively or negatively regulate Shh-target genes, respectively, could not activate caspase-3 (Fig. 3b). As Smo and Ptch1 are transmembrane proteins, whereas Gli1 and Gli3 are signalling mediators that act in the cytoplasm and nucleus, the abnormal activity of Shh signalling at the membrane appears to trigger the elimination of unfit cells.

N-cadherin mediates the sensing of unfit cells

We then explored the mechanisms underlying the elimination of unfit cells. In early embryos, Wnt/ β -catenin signalling post-translationally stabilises E-cadherin, shaping a membrane E-cadherin protein level gradient. Spontaneously emerging Wnt/ β -catenin-unfit cells alter E-cadherin levels, leading to a substantial difference in membrane cadherin levels (cadherin imbalance) between unfit and neighbouring normal cells. This cadherin imbalance stimulates the apoptosis of unfit cells through TGF- β -type Smad activation, ROS production, and Bcl2 protein reduction⁷. We hypothesised that a similar Cadherin-Smad-ROS-Bcl2 system might also be involved in eliminating Shh-unfit cells. N-cadherin (Cdh2) forms a dorsal-to-ventral gradient that inversely correlates with Shh signalling in the developing spinal cord³⁴ (Fig. 4a). Nevertheless, the molecular relationship between N-cadherin and Shh signalling remains unclear. Remarkably, forced activation of Shh signalling by injecting *SmoCA* mRNA or inactivation of Shh signalling by cyclopamine treatment decreased or increased the levels of N-cadherin protein, respectively (Fig. 4b; Supplementary Fig. 3a). Mosaic introduction of Shh-unfit cells overexpressing *SmoCA* or *Ptch1* decreased or increased membrane N-cadherin protein levels, respectively (Fig. 4c). In contrast, neither forced activation nor inhibition of Shh activity affected *n-cadherin* mRNA levels (Supplementary Fig. 3b, c). In addition, unfit-Shh activity did not change *n-cadherin* mRNA levels (Supplementary Fig. 3d). These findings suggest that Shh signalling negatively regulates N-cadherin levels post-translationally. The mosaic introduction of Gli1 or Gli3R did not affect N-cadherin levels (Fig. 4c), suggesting that Shh signalling controls N-cadherin levels through the *Ptch1* and *Smo* receptors but not through transcription factors (Fig. 4d). Unfit Shh activity-induced cadherin imbalance is possibly involved in the sensing of unfit cells. Consistent with this notion, partial N-cadherin knockdown through injecting *n-cadherin* antisense morpholino (MO), which blocks N-cadherin expression^{34,35} (Supplementary Fig. 3e), reduced apoptotic elimination of Shh-high and -low cells (Fig. 4e, f). Moreover, mosaic introduced N-cadherin-overexpressing cells efficiently activated caspase-3 in the N-cadherin-low ventral region (Fig. 4g), indicating that cadherin imbalance sufficiently induces apoptosis. Importantly, partial knockdown of N-cadherin induced unfit cells with ectopic activation and inhibition of *olig2* expression in the developing spinal cord (Supplementary Fig. 3f), which indicates that N-cadherin mediates the elimination of naturally generated unfit cells. Besides N-cadherin, *Cdh11* is also expressed in the developing spinal cord^{34,36}. Partial *Cdh11* knockdown through injecting *cdh11* MO³⁴ did not affect the apoptotic elimination of Shh-unfit cells (Supplementary Fig. 3h). These results indicate that the difference in membrane N-cadherin levels between unfit and neighbouring fit cells is involved in the sensing of Shh-unfit cells.

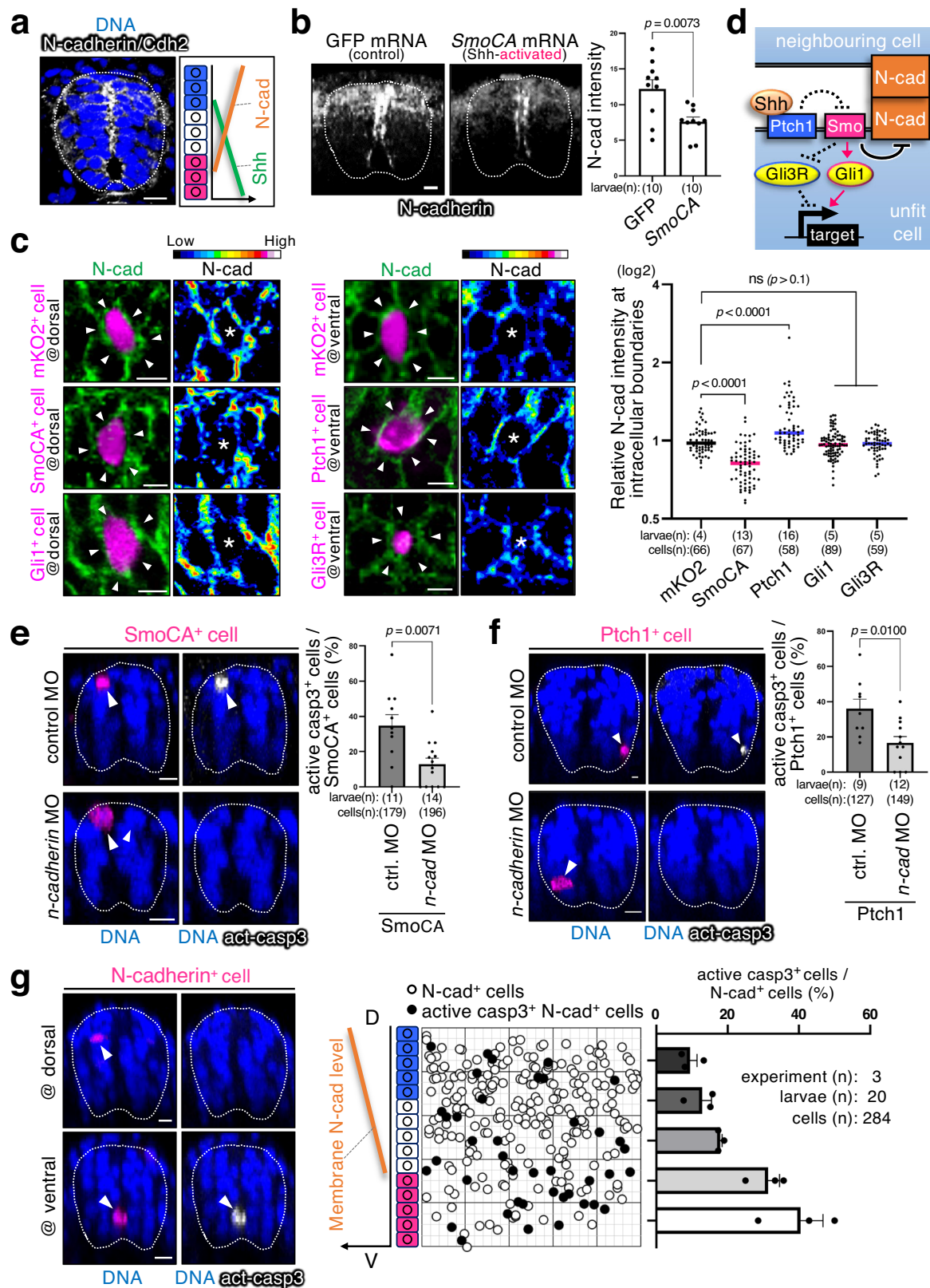
Smad-ROS pathway mediates the killing of Shh-unfit cells

We then examined the involvement of Smad-ROS signalling in the elimination of Shh-unfit cells. SBE-Luc, which expresses luciferase in response to TGF- β -type Smad-dependent signalling, was activated in Shh-high and -low cells in the spinal cord (Fig. 5a) and muscles (Supplementary Fig. 4a). Mosaic introduced N-cadherin-overexpressing cells also activated SBE-Luc (Supplementary Fig. 4b), which indicates that TGF- β -type Smad signalling mediates the killing of unfit cells downstream of cadherin. Inhibiting TGF- β -type Smad signalling by co-expression of Smad3b dominant-negative mutants (Smad3bDN) in unfit cells or injecting *smad4a* MO³⁷ reduced the apoptosis of unfit cells (Fig. 5b, c; Supplementary Fig. 4c, d). Mosaic introduced Shh-high and -low cells triggered DNA oxidation in the spinal cord (Fig. 5d) and muscles (Supplementary Fig. 4e). Treatment with N-acetylcysteine (NAC), a ROS scavenger, prevented cell oxidation (Supplementary Fig. 4f) and cell elimination (Fig. 5e, f; Supplementary Fig. 4g), demonstrating that the Smad-ROS pathway mediates the elimination

of unfit cells (Fig. 5g). Moreover, knockdown of Smad signalling with low dose of *smad4a* MO induced unfit cells with ectopic activation and inhibition of *olig2* expression in the developing spinal cord (Supplementary Fig. 3f), whereas it did not affect the width of *olig2*-expressing area (Supplementary Fig. 3g). These results suggest that Smad signalling mediates the elimination of unfit cells under physiological conditions. In addition, Bcl2 overexpression prevented apoptosis (Fig. 5h, i), suggesting that Bcl2 is involved in the elimination of Shh-unfit cells. Our data collectively demonstrate that cadherin-mediated communication between Shh-unfit and neighbouring fit cells induces apoptosis in unfit cells by activating the Smad-ROS-Bcl2 axis.

Foxo3b is a common mediator of cell competition

We have elucidated that the Cadherin-Smad-ROS-Bcl2 pathway is used in cell competition-mediated elimination of Wnt- and Shh-unfit cells, indicating a common molecular mechanism underlying cell competition. In a previous RNA-seq analysis (GSE133526), we identified *foxo3b*, *sesn3*, *lrx1*, and *tcima* as genes specifically upregulated in unfit cells with abnormally high Wnt/ β -catenin-activity⁷ (Supplementary Table 1). These four genes were upregulated in Wnt/ β -catenin-high unfit cells and Wnt/ β -catenin-low, Shh-high, and Shh-low unfit cells (Fig. 6a, b; Supplementary Fig. 5a, b), which indicates that these genes may be common regulators of the elimination of unfit cells. *foxo3b* encodes a transcription factor^{38,39}, and a Foxo3 target gene *sesn3*⁴⁰ is also upregulated in unfit cells. In addition, a reanalysis of gene set enrichment data in unfit cells (Mosaic β -catCA) compared to control cells (Ubiquitous β -catCA) (GSE133526)⁷ revealed that upregulation of apoptosis-related gene set including *puma* and *apaf1*, which are target genes of Foxo3^{41–46}, was detected in unfit cells (Supplementary Fig. 5c–e; Supplementary Table 2). Therefore, we hypothesised that Foxo3b transcriptional activity may play an essential role in the behaviour of unfit cells. Introduction of the dominant-negative mutant of *foxo3b* (Foxo3bDN) into Wnt- and Shh-defective cells significantly blocked their apoptotic elimination (Supplementary Fig. 6a, b), which suggests that *foxo3b* is essential for their elimination. We also generated *foxo3b* knockout (KO) zebrafish (hereinafter called 'foxo3b-/-') using genome editing (Supplementary Fig. 6c, d). In *foxo3b*-/- mutant, a 4283 bp region, including *foxo3b* exon 1 and 2, was deleted; however, we confirmed that this deletion did not affect the expression of *foxo3b*-neighbouring genes (Supplementary Fig. 6e). As expected, elimination of Wnt- and Shh-unfit cells was blocked in this mutant (Fig. 6c, d). Mosaic introduction of cells expressing a constitutively active Smad3b mutant (Smad3bCA) sufficiently induced *foxo3b* upregulation (Supplementary Fig. 5f). Consistent with the above findings, Smad3bDN co-expression blocked the *foxo3b* upregulation in Shh-unfit cells (Supplementary Fig. 5f), which suggests that *foxo3b* is transcriptionally upregulated downstream of Smad activation. In contrast, ROS inhibition via NAC treatment did not block *foxo3b* upregulation (Supplementary Fig. 5f), but introduction of Foxo3bDN prevented DNA oxidation in Shh-defective cells (Supplementary Fig. 6f). These results suggest that Foxo3b mediates Smad-induced ROS production. To confirm that *foxo3b* transcriptional upregulation occurs upstream of apoptosis induction, we examined the relationship between *foxo3b* and apoptosis inducers, including Puma (p53 upregulated apoptosis inducer)^{41–43} and Caspase-8 (the initiator caspase in extrinsic apoptosis)^{47,48}. The mRNA levels of *puma* were elevated in both β -catCA-expressing (Wnt-high) and Foxo3-hyperactivated cells expressing constitutively active mutants of Foxo3 (Foxo3CA)^{49,50} (Supplementary Fig. 7a), which suggests that *puma* is upregulated downstream of Foxo3 in unfit cells. Consistent with this, artificially introduced Puma and Caspase-8 efficiently induced apoptosis (Supplementary Fig. 7b), but did not lead to *foxo3b* upregulation (Supplementary Fig. 7c). Furthermore, inhibiting apoptosis through *bcl2a* did not impair *foxo3b* upregulation in β -catCA cells (Supplementary Fig. 7c, d). These results indicate that *foxo3b* is activated upstream of



apoptosis induction in unfit cells. Thus, Shh- and Wnt-defective cells are eliminated by activating the Smad-Foxo3-ROS axis.

Next, we examined how *foxo3b* transcription is activated in unfit cells. Because Foxo3 binds to its own promoter and stimulates its expression via a positive auto-regulatory feedback loop in a human cell line⁵¹, we tested the possibility that Foxo3 itself may be involved in

foxo3b transcription in unfit cells. Mosaic introduction of cells-overexpressing wild-type Foxo3 activated endogenous *foxo3b* expression and apoptosis, and mosaic cells-expressing Foxo3CA activated them more strongly (Supplementary Fig. 8a, b). Thus, not only TGF- β -type Smad signalling but also Foxo3 activation can stimulate *foxo3b* expression. Considering these findings together with those of a

Fig. 4 | N-cadherin mediates the sensing of unfit cells. **a** N-cadherin/Cdh2 levels inversely correlate with Shh activity. Representative images show whole-mount immunostaining for N-cadherin (grey). Scale bar = 10 μ m. **b** Activating Shh signalling reduces N-cadherin levels. Shh-activated larvae were prepared by injecting *SmoCA* mRNA. Scale bar = 10 μ m. The mean \pm SEM of N-cadherin intensity of each larva is graphed. An unpaired two-tailed *t*-test was used for the statistical analysis. **c** Mosaic introduction of *SmoCA*- or *Ptch1*-expressing cells altered endogenous N-cadherin levels. Confocal images show whole-mount immunostaining for N-cadherin (green) and mosaic expression of mKO2 alone or with *SmoCA*, *Ptch1*, *Gli1*, or *Gli3R* (magenta). The fluorescence intensity of intercellular N-cadherin staining between mKO2⁺ cells and neighbouring wild-type cells was normalised to the intercellular fluorescence intensity between wild-type cells. Each dot represents an mKO2⁺ cell. Two-tailed one-way ANOVA was used. **d** Schematic illustration of the

Shh signalling pathway and N-cadherin regulation. **e, f** Partial N-cadherin knock-down by injecting low-dose *n-cadherin* oligo morpholino (MO) blocks *SmoCA*- (**e**) or *Ptch1*- (**f**) -expressing cell elimination. Scale bar = 10 μ m. The graphs on the right show the mean \pm SEM of mKO2⁺ (*SmoCA*, *Ptch1*) and caspase-3-active cell frequencies. An unpaired two-tailed *t*-test was used for the statistical analysis. **g** Cells causing excess noise in N-cadherin-gradients efficiently underwent apoptosis. Confocal images show whole-mount immunostaining of mosaic introduced N-cadherin-overexpressing cells (magenta) and active caspase-3 (grey). Scale bar = 10 μ m. The middle panel shows maps of N-cadherin cells artificially introduced into the spinal cord. The right graph indicates the mean \pm SEM of mKO2⁺ and caspase-3-active cell frequencies within a divided range along the DV axis. Source data are provided as a Source Data file.

previous study wherein *Foxo3* and TGF- β -type Smads were reported to form oligomers to control gene expression in the nucleus⁵², raised the possibility that *Foxo3* and TGF- β -type Smads might cooperate to activate *foxo3b* expression in the elimination of unfit cells. Consistent with this notion, both *Smad2* and *Foxo3* were found to be localised in the nucleus of Wnt/ β -catenin-high unfit cells, but not in control cells (Supplementary Fig. 8c). Introduction of *Foxo3bDN* prevented the nuclear translocation of *Smad2* in Wnt/ β -catenin-high unfit cells (Supplementary Fig. 8d). In addition, mosaic introduction of *Foxo3CA* stimulated the nuclear localisation of *Smad2* (Supplementary Fig. 8d). Thus, Smads and *Foxo3* translocate to the nucleus depending on each other's activity in unfit cells. It is likely that downstream of communication between unfit and fit cells, Smads and *Foxo3* are activated, co-translocate into the nucleus, and cooperatively activate the transcription of *foxo3b* in unfit cells. This *foxo3b* expression may enhance *Foxo3* activity via a positive feedback loop and consequently activate the expression of apoptosis inducers, such as *puma* (Fig. 6e).

foxo3b-mediated elimination of unfit cells is essential for precise development

Because unfit cells with abnormal Wnt/ β -catenin, Shh activity, or *dbx1b* expression spontaneously appear during embryogenesis and organogenesis, we also confirmed that *foxo3b* expression was upregulated in naturally generated Wnt-, Shh-, or *dbx1b*-unfit cells (Supplementary Fig. 9a–c). We generated transgenic zebrafish Tg(*foxo3b*:GFP) and Tg(*foxo3b*:mCherry), which expresses GFP or mCherry in cells expressing endogenous *foxo3b* to further examine *foxo3b*-positive unfit cells during development (Supplementary Fig. 9d, e). *foxo3b*-positive cells appeared spontaneously in early embryos (Supplementary Fig. 9f; Supplementary Movie 3) and in the developing spinal cord and muscle primordia (Supplementary Fig. 9g). The number and position of *foxo3b*-positive cells varied among the individuals (Supplementary Fig. 9f, g), indicating that *foxo3b* upregulation is not pre-programmed. Moreover, some *foxo3b*-positive cells activated caspase-3 (Supplementary Fig. 9f, g; Supplementary Movie 3), and the inhibition of apoptosis-induced *foxo3b*-positive cell accumulation (Supplementary Fig. 9h). These results suggest that the *foxo3b* reporter zebrafish can be used to visualise naturally emerging unfit cells which are eliminated through cell competition.

To evaluate the *Foxo3b* function under physiological conditions, we inhibited *Foxo3b* using *foxo3bDN* mRNA. Overexpression of *foxo3bDN* did not affect the expression patterns of Wnt morphogen in early embryos and Shh morphogen in developing organs (Supplementary Fig. 10a, b), whereas it induced accumulation of Wnt signalling-unfit cells (Supplementary Fig. 10c) and ectopic activation or inactivation of a Wnt signalling-target posterior gene *cdx4*⁵³ (Supplementary Fig. 10d) in early embryos, accumulation of Shh signalling-unfit cells (Supplementary Fig. 10e) and ectopic *olig2* activation or inactivation (Supplementary Fig. 10f) in the developing spinal cord, abnormal fast muscle formation (Supplementary Fig. 10g), abnormal

larval morphogenesis (Supplementary Fig. 10h), and poor locomotion (Supplementary Fig. 10i). These results suggest that *Foxo3b* activity is required for the elimination of unfit cells with abnormal morphogen signalling activity and precise morphogenesis. To further confirm physiological *Foxo3b* function, we generated a *foxo3b* KO zebrafish by optimising the CRISPR/Cas9-mediated genome editing system^{54–56} (Supplementary Fig. 11a). We designed four short guide RNAs (sgRNAs) and confirmed that injection of these four sgRNAs, but not of a single sgRNA, induced deletion of the *foxo3b* gene efficiently in F0 generation (hereinafter, referred to as '*foxo3b* KO'). As a control, we injected four sgRNAs targeting *luciferase*, which did not result in any phenotypic abnormalities, to ensure that injection of sgRNAs and Cas9 mix had no side effects (Supplementary Fig. 11a–c). As expected, *foxo3b* KO yielded similar results to those obtained with *foxo3bDN*-mediated inhibition (Fig. 6f–j; Supplementary Fig. 11b, c), suggesting that *foxo3b* upregulation in unfit cells is essential for their elimination and precise tissue patterning (Fig. 6k).

Foxo3 is a universal marker of cell competition

In mice and zebrafish, Ras-hyperactivated cells are physically extruded from the epithelia through competitive communication with neighbouring normal cells^{15,57} and cells expressing high levels of Myc protein kill neighbouring normal cells^{7,10,58}. 'Minute cell competition', which is the most well-documented example of cell competition in *Drosophila* and drives competitive communication between wild-type and ribosomal protein gene *rps3*-mutated cells ('Minute' cells) and consequent apoptotic elimination of mutated cells⁸, can also occur in zebrafish (Fig. 7a, b). Surprisingly, *foxo3b* was upregulated in Minute cells enclosed with normal cells (Fig. 7c), Ras-hyperactivated cells surrounded by normal cells (Fig. 7d) and normal cells neighbouring Myc-high cells (Fig. 7e), all of which are 'loser cells' in cell competition. These results indicate that *foxo3b* is a common marker of loser cells in zebrafish competition.

We next examined whether *Foxo3* is a cell competition marker in mice. Zebrafish have two duplicated *foxo3* copies (*foxo3a* and *foxo3b*), whereas mice only have one (*Foxo3*). Previous phylogenetic and functional analyses revealed that zebrafish *foxo3b* is highly orthologous to mouse *Foxo3*^{39,59,60}. Therefore, we re-analysed the single-cell RNA-seq data of mouse loser cells in post-implantation epiblasts (accession number E-MTAB-80-640)¹². The presumptive loser cells expressed *Foxo3* (Supplementary Fig. 12a, b). We also examined *Foxo3* expression in loser cells with low nuclear YAP levels, which trigger competitive communication with neighbouring normal cells in the mouse pre-implantation epiblast¹¹. Apoptosis inhibition through Z-VAD-FMK treatment increased the number of nuclear YAP-low loser cells in mouse epiblasts (Fig. 7f; Supplementary Fig. 12c–e). *Foxo3* expression levels were low in nuclear YAP-low cells within DMSO-treated epiblasts, but in Z-VAD-FMK-treated epiblasts, *Foxo3* expression levels in nuclear YAP-low loser cells increased, supporting our hypothesis that *Foxo3* is upregulated in loser cells (Fig. 7f;

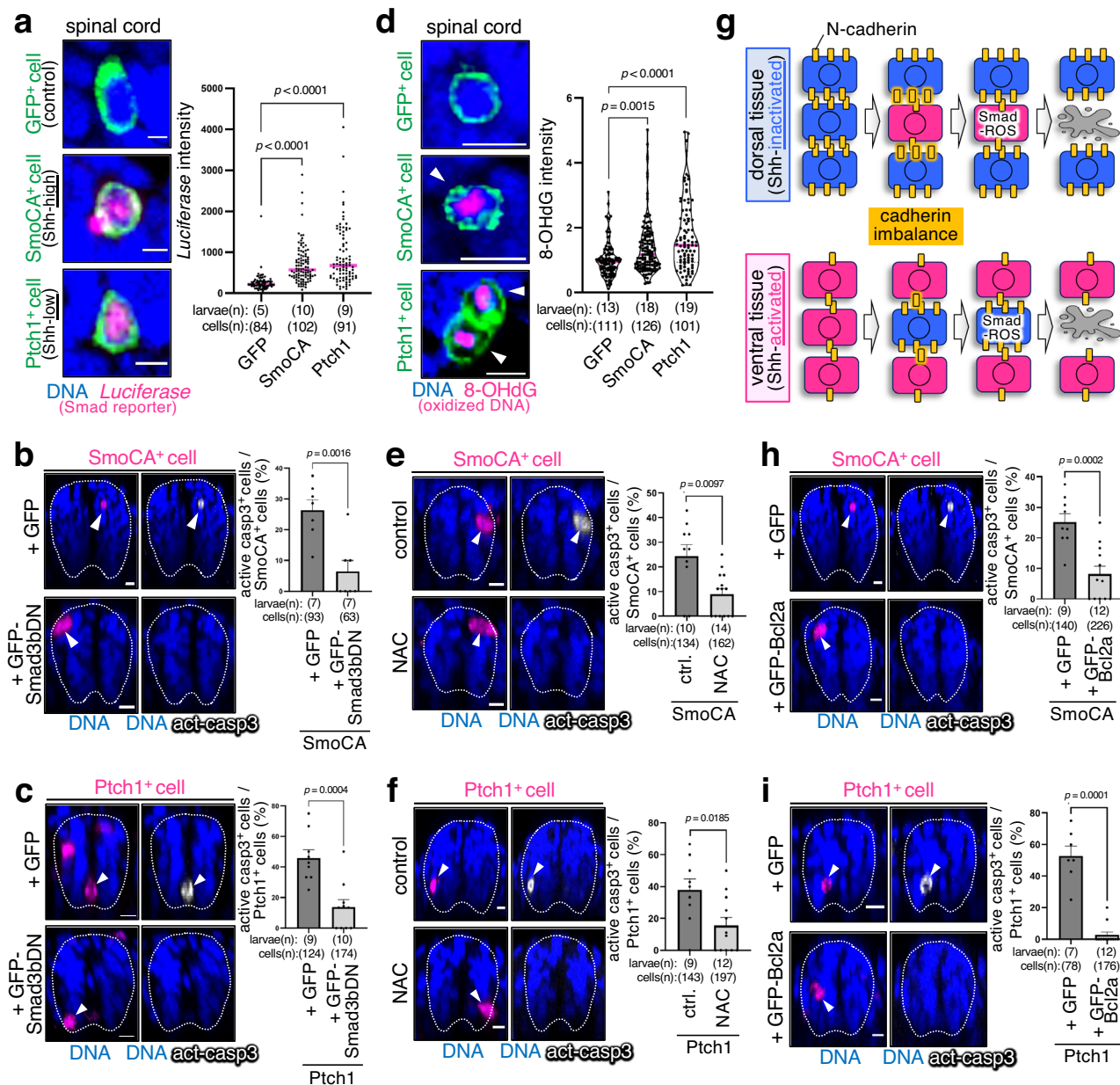


Fig. 5 | Smad-reactive oxygen species pathway mediates the killing of unfit cells. a, d Shh-unfit cells activate the Smad2/3/4-dependent reporter gene (SBE-Luc) (**a**) and reactive oxygen species (ROS) production (**d**). Confocal images show whole-mount fluorescent in situ hybridisation of *luciferase* mRNA (**a**) and immunostaining for 8-OHdG (**d**) (magenta) in mosaic larvae expressing membrane GFP alone or with SmoCA or Ptch1 (green). Scale bar = 10 μ m. In **a**, the *luciferase* intensity of each GFP+ cell is plotted. Two-tailed one-way ANOVA was used. In **d**, violin plots show the 8-OHdG intensity of each GFP+ cell. Two-tailed one-way ANOVA was used. **b, c, e, f, h, i** Smad3bDN overexpression (**b, c**), ROS inhibition

(**e, f**), and Bcl2a overexpression (**h, i**) blocked SmoCA- or Ptch1-expressing cell apoptosis. Confocal images show whole-mount immunostaining of active caspase-3 (grey) in mosaic larvae expressing mKO2 with SmoCA or Ptch1 (magenta), injected with GFP or GFP-Smad3bDN (**b, c**), treated with D2W (control) or N-acetyl-L-cysteine (NAC, a ROS scavenger) (**e, f**), or injected with GFP or GFP-Bcl2a (**h, i**). Scale bar = 10 μ m. The graphs on the right show the mean \pm SEM of mKO2+ (SmoCA, Ptch1) and caspase-3-active cell frequencies. An unpaired two-tailed *t*-test was used for the statistical analysis. **g** Schematic diagram showing the elimination of Shh-unfit cells. Source data are provided as a Source Data file.

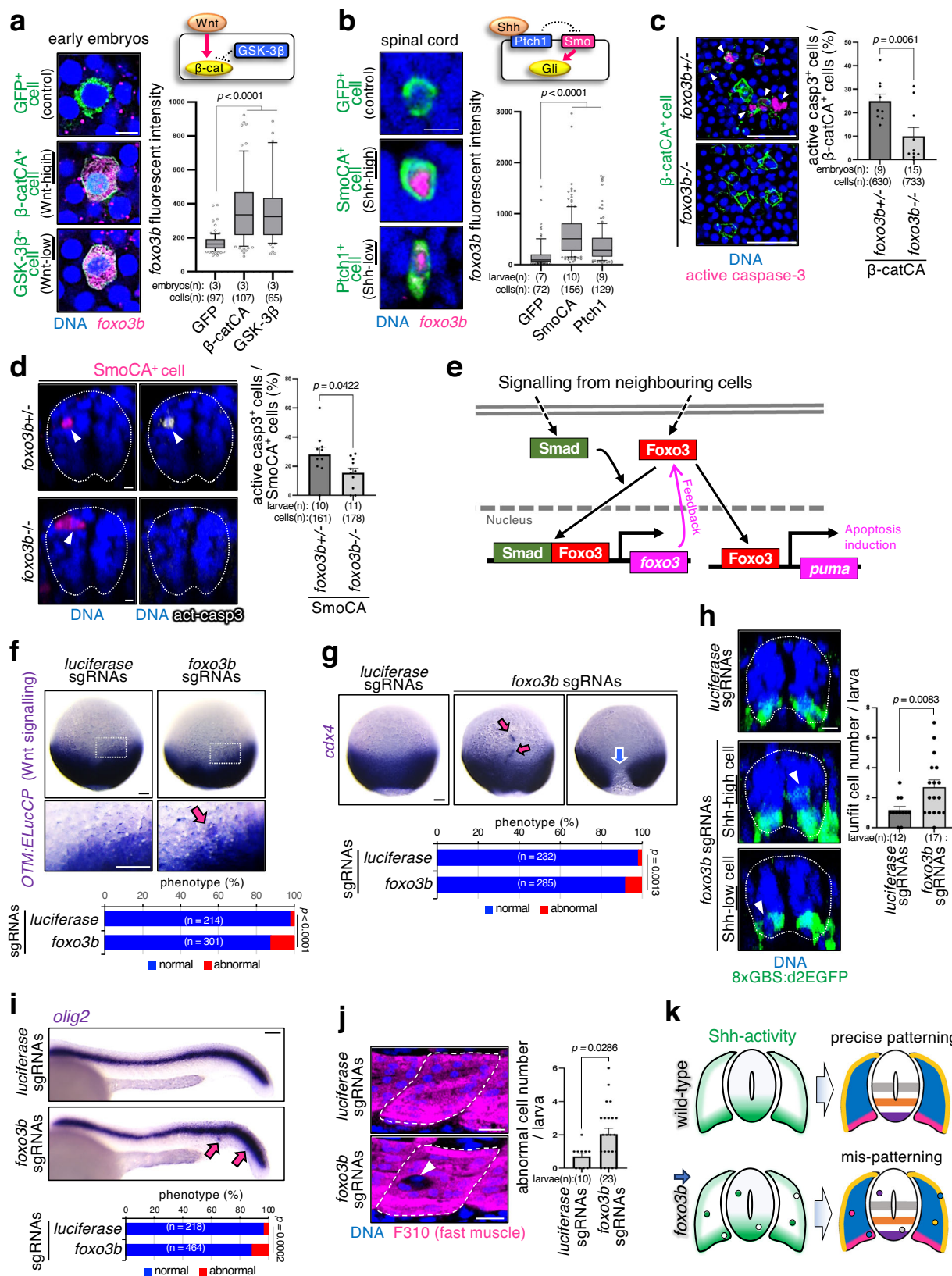
Supplementary Fig. 12c–g). Thus, Foxo3 may be a universal marker for less-fit cells in various cell competition contexts.

Discussion

In this study, we identified a previously unknown universal cell competition marker in vertebrates and elucidated the novel roles and mechanisms of physiological cell competition during organogenesis—the Shh-unfitness-driven cell competition. In zebrafish spinal cord and muscle development regulated by Shh morphogen gradients, unfit cells with abnormal Shh activity spontaneously appear and distort the morphogen gradient. Subsequently, unfit cells alter membrane

N-cadherin levels, activate the Smad-Foxo3-ROS axis, and undergo apoptosis through communication with neighbouring normal cells. In zebrafish and mouse, Foxo3 is upregulated in cells with abnormal morphogen signalling and in various less-fit cells, which are eliminated through cell competition. Thus, Foxo3 can be a common marker of cell competition in vertebrates.

Artificially introduced cells with abnormal Myc or Axin2 activity trigger competitive communication with neighbouring normal cells in developing mouse organs (i.e. the heart, skin, and brain)^{61–63}. These facts suggest that developing tissues can eliminate unfit cells through cell competition. However, whether unfit cells are generated and drive



cell competition during physiological organogenesis is poorly understood. This is partly due to the inherent difficulty in capturing spontaneously arising abnormal cells. In our zebrafish model, which is well-suited for imaging analyses, we previously captured the emergence of unfit cells during embryogenesis⁷. In this study, we visualised abnormal cell appearance and endogenous cell competition in vertebrate

organogenesis and elucidated their regulatory mechanisms. Furthermore, we demonstrated that eliminating these unfit cells is essential for proper organogenesis. Thus, we have revealed the physiological significance of cell competition during organogenesis.

Drosophila imaginal discs, which form bone morphogenetic protein (BMP) morphogen gradients, can eliminate artificially introduced

Fig. 6 | Foxo3b is a common marker of cell competition. Artificially introduced Wnt-unfit cells into early embryos (9 hpf) (**a**) and Shh-unfit cells in the developing spinal cord (24 hpf) (**b**) strongly express *foxo3b*. Confocal images show whole-mount fluorescent in situ hybridisation of *foxo3b* mRNA (magenta) in GFP alone or with β -catCA, GSK-3 β , SmoCA, or Ptc1 (green). *foxo3b* intensity of each GFP⁺ cell was graphed. Maximum and minimum: whiskers; medians: lines; 10th and 90th percentiles: boxes. Two-tailed one-way ANOVA was used. **c, d** Eliminating Wnt- and Shh-unfit cells require *foxo3b*. Representative confocal images show mosaic embryos expressing GFP-tagged β -catCA (green), mKO2-tagged SmoCA (magenta), and active caspase-3 (magenta in **c**), grey in **d**) in *foxo3b* heterozygous (*foxo3b*^{+/−}) or homozygous (*foxo3b*^{−/−}) mutants. The graph on the right shows the mean \pm SEM of β -catCA⁺ or SmoCA⁺, caspase-3 active cell frequencies. An unpaired two-tailed *t*-test was used for the statistical analysis. **e** Schematic illustration of the Smad-Foxo3 signalling. **f, h** *foxo3b* inhibition enhances Wnt- and Shh-unfit cell accumulation. Whole-mount in situ hybridisation of *ELuc* in Tg(OTM:ELucCP) embryos (**f**) or

immunostaining of d2EGFP (green) in Tg(8xGBS:d2EGFP) larvae (**h**) injected with *luciferase* or *foxo3b* sgRNAs (*foxo3b* KO). The bar plots show unfit cell frequencies in each sample. The chi-square test and an unpaired two-tailed *t*-test were used for statistical analyses in (**f, h**), respectively. **g, i, j** *foxo3b*-mediated unfit cell elimination is required for precise tissue patterning. Representative images show the whole-mount in situ hybridisation of *cdx4* (**g**) or *olig2* (**i**) and immunostaining for fast myosin (**j**) injected with *luciferase* or *foxo3b* sgRNAs. The bottom graph in (**g, i**) show the percentages of embryos/larvae with normal or abnormal expression patterns. The chi-square test was used for statistical analysis (**g, i**). The graph to the right of **j** shows the mean \pm SEM of abnormal gene expressing-cell frequencies in each larva. An unpaired two-tailed *t*-test was used for the statistical analysis. **k** Precise morphogen gradient formation and tissue patterning require *foxo3b* activity. Scale bar = 10 μ m in (**a, b, d, h, j**), and 100 μ m in (**c, f, g, i**). Source data are provided as a Source Data file.

cells with abnormally high or low BMP activity^{64,65}. Zebrafish embryonic tissue eliminates naturally and artificially generated cells with unfit Wnt/ β -catenin signalling activity through cell competition to correct noisy Wnt/ β -catenin morphogen gradients and achieve precise anterior–posterior patterning⁷. This study demonstrates that cell competition-mediated elimination of Shh-unfit cells ensures the precise Shh morphogen gradient formation and robust spinal cord and muscle patterning. These findings indicate that cell competition-mediated morphogen gradient correction may function irrespective of the morphogen type, supporting robust tissue patterning. Because morphogen gradients are also formed in adult organs^{66–68}, this correction system may be involved in tissue homeostasis and regeneration. Regarding the elimination mechanisms, Wnt- and Shh-unfit cells are eliminated via cadherin-mediated communication with neighbouring fit cells and activation of the Smad-Foxo3-ROS axis. However, how Shh morphogen signalling controls N-cadherin levels remain elusive. As N-cadherin levels are regulated in the plasma membrane, investigating the endocytic processes of cadherins may offer intriguing perspectives. It might be interesting to focus on Cell-adhesion molecule-related/down-regulated by Oncogenes (Cdon) protein as a possible mediator of this process because Shh signalling negatively regulates Cdon expression, and Cdon positively regulates membrane-localisation of N-cadherin in developing zebrafish spinal cord⁶⁹. Thus, our studies indicate that dose-dependent morphogen signalling activation in morphogen-receiving cells and cadherin-mediated inter-cellular coordination is required to precisely form morphogen gradients and consequent tissue patterns.

In addition to cell competition, cadherin-mediated cell sorting contributes to morphogen gradient correction during spinal cord development in zebrafish³⁴. In the spinal cord, strong Shh signalling activation induces protocadherin 19 (Pcdh19) transcription, whereas moderate Shh signalling levels induce the transcriptional activation of type-II cadherin Cdh11. Because of this Shh activity-dependent cadherin transcription and preferential homophilic cadherin binding, cells with unfit Shh activity migrate to areas with fitter Shh activity³⁴. However, the significance of multiple systems for morphogen gradient correction and differential utilisation in developing tissues is unknown. To clarify this, identifying specific regulatory factors governing cell sorting is critical.

In this study, we demonstrated that cell competition is crucial for robust spinal cord development by inhibiting cell competition through the blocking of apoptosis or *foxo3* activity. Furthermore, forced inhibition of cell competition led to the accumulation of Shh-high cells in the Shh-high ventral region (Supplementary Figs. 4h, 6g), indicating that ectopically generated and surviving Shh-high cells may have migrated to the Shh-high fit area. This finding also suggests that cell competition and sorting-mediated systems mutually influence one another. Considering the efficient activation of the apoptosis-mediated system in cells only causing substantial

noises in morphogen gradients, the ‘unfitness’ of unfit cells can determine the system they use. For example, minor and fluctuating noise may be repaired by sorting, whereas severe and persistent noise may be eliminated through cell competition. Notably, the types of cadherins and their regulatory mechanisms differ between these two systems. Cdh11 and Pcdh19, which are transcriptionally regulated by the Shh morphogen gradient, mediate sorting³⁴, whereas N-cadherin, which is post-translationally regulated by the Shh morphogen, mediates cell competition. Investigating this distinction may provide insights into the underlying switching mechanisms.

The universal mechanisms regulating diverse types of cell competition remain unknown. Transcriptomic analysis indicated that the Flower-Azot pathway is specifically activated in loser cells in *Drosophila*^{16,17}. However, our previous RNA-seq data did not show upregulation of *flower* or *azot*-like genes in Wnt-unfit cells (GEO accession code: GSE133526)⁷ (Supplementary Table 1), which indicates that the Flower-Azot pathway might not be a universal machinery of cell competition in vertebrates. This study identified several genes encoding common regulator candidates, including *foxo3b*, *sesn3*, *tcima*, and *lnx1*. *foxo3b* is commonly upregulated in cells that lose cell competition driven by Wnt, Shh, Ras, Myc, and ribosomal proteins in zebrafish. In addition, less-fit cells in mice also had upregulated *Foxo3*, suggesting that Foxo3 is a potential universal marker of cell competition in vertebrates.

However, how different cellular fitness leads to *foxo3* expression in unfit cells, and what is the specific functional role of Foxo3 in each context is still unclear and requires further investigation. This study shows that, at least in unfit cells with abnormal Wnt signalling activity, Smads and Foxo3 apparently translocate into the nucleus cooperatively and activate the expression of *foxo3*. A similar mechanism would be used in the apoptosis of Shh-unfit cells because Smad activation and *foxo3* upregulation are required for this process. On the contrary, we previously showed that Myc-mediated cell competition occurs in a Smad-independent manner⁷. It is well-known that Foxo family proteins can associate with a variety of unrelated transcription factors to regulate the expression of target genes^{70–72}. Therefore, it would be interesting to investigate the possibility of Foxo3 binding to different transcription factors depending on the type of cellular unfitness, thereby inducing *foxo3* expression in the nucleus.

Because less-fit cells appear sporadically, analysing when and where cell competition occurs is challenging. In this study, we generated a Tg(*foxo3b*:GFP) and Tg(*foxo3b*:mCherry) reporter to visualise the spatiotemporal dynamics of *foxo3b* expression from embryogenesis to organogenesis, which enabled us to understand the spatiotemporal dynamics and roles of physiological cell competition. However, Foxo3 is involved in various signalling pathways (e.g. cell metabolism, DNA damage repair, and stress resistance)^{38,73}, and

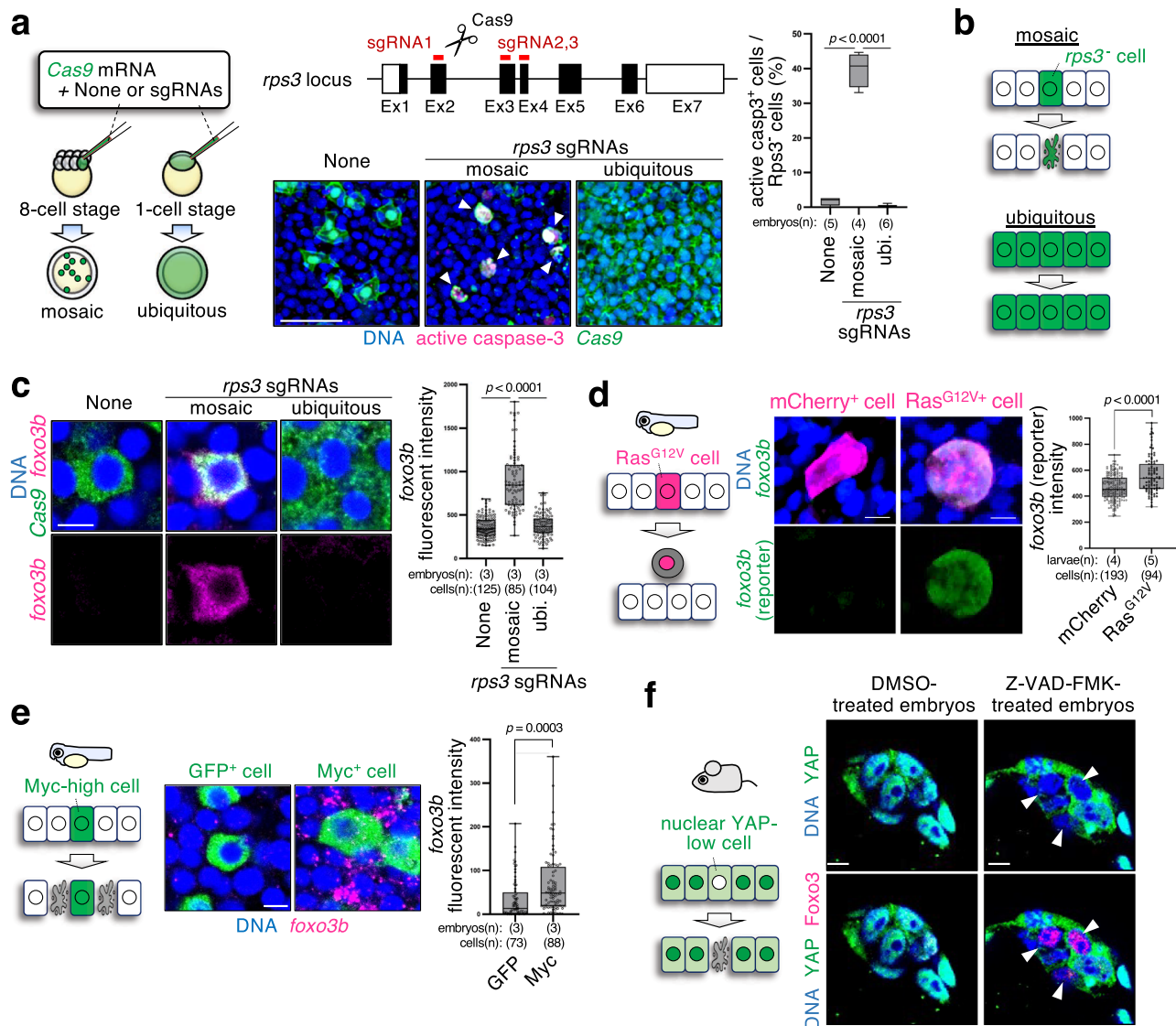


Fig. 7 | Foxo3 is a universal marker of cell competition. **a** Cell competition eliminates *rps3* mutant cells. The schematic diagram on the left shows the experimental introduction of *rps3* mutant cells into zebrafish embryos in a mosaic or ubiquitous manner using CRISPR/Cas9-mediated genome editing. Confocal images show whole-mount immunostaining of embryos (9 hpf) without *rps3* mutants (none) or with mosaic or ubiquitous *rps3* mutants (green) and active caspase-3 (magenta). Scale bar = 100 μ m. The box plot on the right shows the mean \pm SEM of the *foxo3b* intensity of each GFP⁺ cell (c), mCherry⁺ cell (d), and cells neighbouring GFP⁺ cell (e). Maximum and minimum: whiskers; medians: lines; 25th and 75th percentiles: boxes. Two-tailed one-way ANOVA was used. **b** Schematic illustration indicating that *rps3* mutant cells are eliminated by competition with neighbouring normal cells. **c** *rps3* mutant cells upregulate *foxo3b*. Representative images show whole-mount in situ hybridisation of *foxo3b* mRNA (magenta) in embryos without *rps3* mutants (none) or with mosaic or ubiquitous *rps3* mutants (green). Scale bar = 10 μ m. **d** Oncogenic Ras^{G12V} cells show upregulated *foxo3b* expression. Confocal images show endogenous *foxo3b* (green)

expression in Tg(*foxo3b*:GFP) 24 hpf larvae expressing mCherry alone or with Ras^{G12V}. Scale bar = 10 μ m. **e** Myc-surrounding cells upregulate *foxo3b*. Myc-high cells communicate with and induce apoptosis in the surrounding Myc-low cells. Representative images show whole-mount in situ hybridisation of *foxo3b* mRNA (magenta) in mosaic embryos (9 hpf) expressing GFP alone or with Myc. Scale bar = 10 μ m. In the box plot on the right shows the mean \pm SEM of the *foxo3b* intensity of each GFP⁺ cell (c), mCherry⁺ cell (d), and cells neighbouring GFP⁺ cell (e). Maximum and minimum: whiskers; medians: lines; 25th and 75th percentiles: boxes. An unpaired two-tailed one-way ANOVA was used. **f** Nuclear YAP-low loser cells in mouse pre-implantation epiblast express Foxo3. Representative images show whole-mount immunostaining for YAP (green) and Foxo3 (magenta) in DMSO-treated (control) or Z-VAD-FMK-treated (apoptosis-inhibited) embryos. Note that most of the cells in DMSO-treated embryos are nuclear YAP-high and Foxo3-low, but Z-VAD-FMK treatment increased nuclear YAP-low and Foxo3-high cells. Scale bar = 10 μ m. Source data are provided as a Source Data file.

therefore, to attain a more accurate understanding of physiological cell competition, integrating additional factors, such as *sesn3*, *tcima*, *lnx1*, would be advantageous. This approach would allow us to precisely detect naturally generated unfit cells, and thereby help understand the importance of physiological cell competition and elucidate the causes of the ‘abnormality’ of unfit cells.

Cells with abnormal Shh and Wnt signalling activities or Foxo3 dysregulation can be the origin of tumorigenesis^{74–79}. Therefore, cell competition-mediated elimination of unfit cells might support robust tissue development and serve as a mechanism to suppress cancer

initiation. Additionally, Foxo3 is well known for its association with ageing and age-related diseases. For instance, genetic variations in Foxo3 are associated with longevity^{80–82}, whereas the decreased activity of Foxo3 is implicated in the progression of age-related diseases⁸³. We also show that some *foxo3b*^{-/-} zebrafish, which appeared phenotypically normal during embryonic and larval development, exhibited deformities as they aged (Supplementary Fig. 11d). Foxo3 may sustain the robustness of tissue homeostasis via cell competition throughout life. Interestingly, a previous study reported that *foxo3b*-null zebrafish have lower survival rates under hypoxic stress⁸⁴.

Possibly, this vulnerability to hypoxia might partly be due to poor-quality cells, which would normally be removed through cell competition, persisting in these *foxo3*-deficient zebrafish. Thus, it would be interesting to investigate the role of this system in health maintenance, stress tolerance, and prevention of ageing. Our findings reveal a novel facet of Foxo3 that has already been recognised as an anti-ageing factor.

Methods

Ethical approval

All experimental animal care was performed following institutional and national guidelines and regulations. The study protocol was approved by the Institutional Animal Care and Use Committee of Osaka University (RIMD Permit# Biken-AP-R02-04, FBS Permit# FBS-20-001). The study was conducted following the ARRIVE guidelines.

Zebrafish maintenance

Adult zebrafish were maintained under a 14 h light/10 h dark cycle at 28.5 °C. Wild-type strains (AB) and the following transgenic lines were used: Tg(8xGBS:d2EGFP)³², Tg(OTM:ELuc-CP)⁷, Tg(hsp70l:mKO2-T2A-SmoCA), Tg(hsp70l:GFP-zBcl2a), Tg(*foxo3b*:GFP), Tg(*foxo3b*:mCherry), *foxo3b*^{-/-}, and Tg(*krt4p:gal4*)⁸⁵. One-cell stage embryos were used for cell injection to generate transgenic fish or mosaic embryos and larvae, with the larvae processed at 24 h post-fertilisation (hpf).

Plasmids

8xGBS:d2EGFP was constructed by inserting the Smal fragment of 8×3' Gli-BS-δS1-LucII⁸⁶, including the Gli-binding sequence (Gli-BS), between the Tol2 excision site and a minimal promoter (miniP, AGAGGGTA-TATAATGGAAGCTCGACTTCCAG), derived from pGL4 (Promega, Madison, WI, USA), of XhoI/EcoRI-digested pT2-TCF-mini-d2EGFP⁸⁷. The half-life of d2EGFP protein, which was used as a fluorescent reporter in 8xGBS:d2EGFP, is relatively short (approximately 2 h), and this property facilitated the detection of dynamic changes during Shh signalling *in vivo*.

The *hsp70l* promoter was sub-cloned into a pTol2 vector (a gift from Dr K. Kawakami) to prepare heat-shock promoter-driven plasmids. mKO2 or membrane-tagged (GAP43-fused) GFP and T2A were then sub-cloned into the pTol2-*hsp70l* promoter plasmid. These plasmids expressed mKO2 or GAP43-GFP in response to heat shock. PCR-amplified cDNA encoding signalling modulator proteins were sub-cloned downstream of T2A in pTol2-*hsp70l*:mKO2 (or GAP43-GFP)-T2A plasmids to generate plasmids expressing mKO2 or GAP43-GFP with signalling modulator proteins.

The Shh signalling activators included a constitutively active mutant of mouse Smoothened (SmoCA), in which Trp539 was replaced with Leu (a gift from Dr P. Beachy, Addgene plasmid #37673; Cambridge, MA, USA)⁸⁸ and human wild-type Gli1 (a gift from Dr B. Vogelstein; Addgene plasmid #16419)⁸⁹. Shh signalling inhibitors included mouse wild-type Ptc1 (a gift from Dr P. Beachy, Addgene plasmid #120889)⁹⁰ and the dominant-negative form of Gli3R (a gift from Dr B. Vogelstein; Addgene plasmid #16420)⁸⁹. Other signalling regulators were as follows: N-cadherin; Smad3bDN, in which Pro401, Ser421, and Ser423 were substituted with His, Ala, and Ala, respectively⁹¹; constitutively active zebrafish Smad3b mutant (Smad3bCA), in which Ser421 and Ser423 were substituted with Asp; *foxo3b*DN (N-terminus-truncated zebrafish *foxo3b*)⁹²; mouse wild type Foxo3 (Foxo3WT); constitutively active mouse Foxo3 (Foxo3CA), in which Thr32, Ser252, and Ser314 were substituted with Ala; GFP-fusion zebrafish Bcl2a (GFP-Bcl2a); human Puma (a gift from Dr B. Vogelstein; Addgene plasmid #16588)⁴³; and zebrafish Caspase-8. Wnt/β-catenin signalling activator (N-terminus-truncated mouse β-catenin, β-catCA) and Wnt/β-catenin signalling inhibitor (human wild-type GSK-3β) have been described previously⁷. To prepare UAS promoter-driven plasmids expressing constitutively active human

H-Ras (Ras^{G12V}) mutants, Gly12 was substituted with Val (pTol2-UAS-mCherry-T2A-Ras^{G12V}), as described previously¹⁵.

cDNAs for signalling proteins were PCR-amplified and cloned into the multi-cloning site of the pCS2p+ vector for mRNA synthesis. The cloned proteins were caspase activity fluorescent biosensor/CC3Ai (a gift from Dr. B. Li, Addgene #78909)⁹³, mScarlet (a gift from Dr D. Gadella, Addgene plasmid #85042)⁹⁴, GFP, Cas9, human Bcl2a (a gift from Dr S. Korsmeyer, Addgene #8768)⁹⁵, mouse SmoCA, and zebrafish Foxo3b and Smad2.

sgRNA synthesis

We selected target sequences for each gene that did not overlap with other genomic sequences using the CRISPR design tool CHOPCHOP. The protocol for sgRNA synthesis was based on a previously reported method⁹⁶. The oligonucleotides containing a T7 promoter sequence, target sequence, and the sgRNA templates were PCR-amplified from sgRNA scaffold oligo⁹⁷ using the oligonucleotides and primer sgRNA-RV with PrimeSTAR Max (TaKaRa, Kusatsu, Japan) and purified using the NucleoSpin Gel and PCR Clean-up Kit (MACHEREY-NAGEL, Düren, Germany). sgRNAs were synthesised using the CUGA7 gRNA Synthesis Kit (Nippon Gene, Tokyo, Japan), and their concentrations were measured using a NanoDrop Lite spectrophotometer (Thermo Fisher Scientific, Waltham, MA, USA).

Generation of transgenic zebrafish

Plasmid DNA and Tol2 transposase mRNA were co-injected into one-cell stage wild-type zebrafish embryos to generate Tg(*hsp70l*:mKO2-T2A-SmoCA) and Tg(*hsp70l*:GFP-zBcl2a) zebrafish. To generate Tg(*foxo3b*:GFP) and Tg(*foxo3b*:mCherry) zebrafish, a donor plasmid containing a heat-shock promoter was co-injected into one-cell stage wild-type embryos with a sgRNA targeted for genome digestion, an sgRNA targeted for donor plasmid digestion, and the Cas9 protein (MO646, New England Biolabs, Ipswich, MA, USA)⁹⁸. The sgRNA sequences were 5'-tcccgtacgcggatccaggggg-3' (*foxo3b* transcription start site (TSS) upstream target) and 5'-ggctgctgcaggagctcatgg-3' (tbait).

Two sgRNAs and Cas9 were co-injected into one-cell-stage wild-type embryos to generate *foxo3b*^{-/-} zebrafish. Two gRNAs were designed to delete the 2 kb upstream promoter region from the TSS and exon 2. The sgRNA sequences were as follows: 5'-catgctcaacataggacagtg-3' (-2 kb from the TSS) and 5'-gaactgctgctgtgcacagg-3' (flanking region of exon2). Transgenic fish were then outcrossed with wild-type fish to produce founder lines. Heterozygous adult fish were crossed to obtain homozygous transgenic lines.

Clonal introduction of Shh-unfit cells

H2B-mCherry (100 pg) mRNA, with or without *SmoCA* mRNA (400 pg), was injected into two blastomeres of an eight-cell stage embryo. This method introduces Shh-unfit cells at the patchy-clone level.

Mosaic introduction of Shh-unfit cells

Hsp70 promoter-driven plasmids (12.5–50 pg) were injected into one-cell stage embryos and maintained at 23.5 °C until 14 hpf (10-somite stage). After bringing larvae back to 28.5 °C for 15 min, they were transferred to pre-warmed egg water at 37 °C and kept at this temperature for 1 h to expose them heat shock. Subsequently, larvae were placed at 28.5 °C and then fixed at 24 hpf for immunostaining or *in situ* hybridisation. This method introduces Shh-unfit cells at the single-cell level but not at the patchy-clone level.

Mosaic introduction of Wnt-unfit cells

Hsp70 promoter-driven plasmids (5–17.5 pg) were injected into one-cell stage embryos and maintained at 28.5 °C until 4.3 hpf (dome stage). The embryos were then exposed to heat-shock at 37 °C for 1 h. After the heat shock, embryos were placed at 28.5 °C and then fixed at 9 hpf.

Mosaic introduction of oncogenic cells

UAS promoter-driven plasmids (7.5–25 µg) were injected into one-cell stage Tg(*krt4p:gal4*) embryos, maintained at 25.5 °C and then fixed at 26–28 hpf.

foxo3b KO zebrafish in F0 generation

Cas9 and four sgRNAs were injected into one-cell stage embryos to generate *foxo3b* KO zebrafish in F0 generation^{54–56}. The sgRNA sequences were as follows: 5′-ccggcgaaggccaaaatgggg-3′, 5′-gacg-gaggctcccgccgaagg-3′, and 5′-ggattcagaacccatttttgg-3′, 5′-gcgtagacgtagttttgagagg-3′. As control, four *luciferase* sgRNAs were injected; their sequences were as follows: 5′-gggcatttcgcagcctaccgtgg-3′, 5′-ggcatgcgagaatctcagcagg-3′, and 5′-tcggggaagcggttccaagg-3′, and 5′-ttgtggacgaagtaccgaaagg-3′.

Mosaic or ubiquitous introduction of *rps3* mutant cells

Cas9 mRNA and sgRNAs were injected into a single blastomere of an eight-cell stage embryo to introduce mosaic mutants⁹⁹. Cas9 mRNA and sgRNAs were injected into one-cell stage embryos to generate ubiquitous mutants⁹⁹. Three sgRNAs were injected to disrupt the *rps3* gene efficiently^{54,56}. The sgRNA sequences were as follows: 5′-cgaggatgggtattccggcgtgg-3′, 5′-cattcgtgagctgaccgctgtgg-3′, and 5′-tctctgcgtcaacgctgctcgg-3′.

Time-lapse imaging and data analysis

For time-lapse confocal live imaging, larvae with mosaically introduced SmoCA cells (Supplementary Movie 1, 2) or Tg(*foxo3b:mCherry*) embryos (Supplementary Movie 3) were manually dechorionated using forceps and mounted in 1% low melting agarose with egg water onto glass bottom dishes. Live imaging was performed using an FV3000 confocal laser scanning microscope (Olympus, Tokyo, Japan). In Supplementary Movie 1, 2, two laser lines at 488 and 594 nm were used. The recording interval was 10 min. At each time point, 30 confocal slices were acquired along the z-axis. In Supplementary Movie 3, three laser lines at 445, 488, and 561 nm were used. The recording interval was 10 min. At each time point, 18 confocal slices were acquired along the z-axis.

Antibodies

Primary antibodies included anti-fast myosin (F310) (#AB_531863, 1/10; Developmental Studies Hybridoma Bank (DSHB), Iowa City, IA, USA); anti-slow myosin (F59) (#AB_528373, 1/10; DSHB); anti-muscle pioneer (4D9) (#AB_528224, 1/5; DSHB); anti-N-cadherin (Cadherin2) (#125885, 1/1000; GeneTex, Irvine, CA, USA); chicken anti-GFP (#13970, 1/1000; Abcam, Cambridge, UK); rabbit anti-GFP (#A-11122, 1/500; Thermo Fisher Scientific); anti-active caspase-3 (#559565 (1/500; BD Bioscience, Franklin Lakes, NJ, USA) and #9661 (1/500; Cell Signalling, Mountain View, CA, USA)); and anti-V5 tag (R960-25, 1/200; Invitrogen).

Secondary antibodies included AlexaFluor488-conjugated anti-chicken IgY (#A-78948, 1/1000; Invitrogen, Waltham, MA, USA) and anti-rabbit IgG (#A-11034, 1/500; Invitrogen); AlexaFluor594-conjugated anti-mouse IgG (#A-11032, 1/500; Invitrogen) and anti-rabbit IgG (#A-11037, 1/500; Invitrogen); AlexaFluor647-conjugated anti-rabbit IgG (#4414, 1/500; Cell Signalling Technology); and anti-mouse IgG (#A-21235, 1/500, Invitrogen).

mRNA and antisense oligo MO microinjection

Capped mRNA was synthesised using the SP6 mMESSSEAGE mMA-CHINE kit (Ambion, Austin, TX, USA) and purified using Micro Bio-Spin columns (Zymo Research, Irvine, CA, USA). The synthesised mRNA was injected into one-cell-stage embryos. Antisense oligo MOs (Gene Tools, Philomath, OR, USA) were injected into one-cell stage embryos to perform knockdown experiments in zebrafish larvae. Standard control morpholino, 5′-CCT CTT ACC CTC AGT TAC AAT TTA TA-3′;

N-cadherin (*n-cadherin*)^{34,35}, 5′-TCT GTA TAA AGA AAA GCG ATA GAG TT-3′ (1 ng); Smad4 (*smad4a*)³⁷, 5′-AAT CAT ACT CAT CCT TCA CCA TCA T-3′ (2 ng); and Cadherin11 (*cdh11*)³⁴, 5′-TCT GTA TAA AGA AAC CGA TAG AGT T-3′ (2 ng) were injected. *n-cadherin* and *smad4a* MOs are translation-blocking morpholinos, and *cdh11* MO is a splicing-blocking morpholino. We adjusted the concentration of the MOs to achieve a level of expression that was sufficiently reduced without causing severe morphogenetic defects.

Chemical treatment

Zebrafish larvae were treated with 30 µM Smo inhibitor, cyclopamine (Selleck Chemicals, Houston, TX, USA), to downregulate the Shh signalling activity. Larvae were treated with 100 µM NAC (Sigma-Aldrich, St. Louis, MO, USA) to evaluate the effects of ROS on eliminating unfit cells. Each solution was added at 18 hpf.

Whole-mount immunostaining

At 9 hpf, embryos were fixed with pre-cooled 4% paraformaldehyde in phosphate-buffered saline (PBS) overnight at 4 °C. At 24 hpf, larvae were dechorionated with 1 mg/mL pronase (Roche, Darmstadt, Germany) and fixed with 4% paraformaldehyde in PBS overnight at 4 °C. The embryos and larvae were washed with 0.5% Triton X-100 (PBST) at least four times and blocked with 10% foetal bovine serum, 4% Block Ace (Megmilk Snow Brand, Tokyo, Japan), and 1% dimethylsulphoxide (DMSO) in 0.1% PBST for 1 h. The embryos and larvae were incubated with the primary antibodies overnight at 4 °C, washed, and incubated with AlexaFluor-conjugated secondary antibodies with Hoechst33342 (H3570, 1/1000; Invitrogen) overnight at 4 °C.

Immunostaining for anti-8-OHdG was performed as described previously, with slight modifications¹⁰⁰. Larvae were dechorionated at 24 hpf with 1 mg/mL pronase and fixed with pre-cooled 50% Bouin's solution in PBS overnight at 4 °C. The larvae were washed with 0.5% PBST at least 12 times. After rinsing with 0.5% PBST, larvae were treated with 0.1% collagenase in 2% PBST at 28.5 °C for 15 min. After rinsing with 0.5% PBST, larvae were treated with proteinase K (10 µg/mL) at 28.5 °C for 12 min. After rinsing with 0.5% PBST, DNA was denatured using 4 N HCl for 12 min at 28.5 °C. The pH was adjusted with 50 mM Tris-HCl for 5 min at 28.5 °C. After rinsing with 0.5% PBST and blocking, larvae were incubated with anti-8-OHdG monoclonal antibody (15A3, sc-66036, 1/100; Santa Cruz Biotechnology, Dallas, TX, USA) and anti-GFP antibody overnight at 4 °C, and then washed and incubated with AlexaFluor-conjugated secondary antibodies and Hoechst33342 overnight at 4 °C. Stained larvae were visualised using an FV3000 confocal laser scanning microscope. Images were prepared and analysed using ImageJ software (NIH, Bethesda, MD, USA).

Whole-mount in situ hybridisation

RNA probe synthesis was performed as described previously¹⁰¹. The probes used were as follows: *n-cadherin*, *dbx1b*, *olig2*, *foxa2*, *cdx4*, *foxo3b*, *sesn3*, *lnx1*, *tcima*, *puma*, *wnt8a*, *shh*, *GFP*, *Emerald luciferase* (ELuc), and *firefly luciferase* (Luc). SBE-Luc (pGL4.48[luc2P/SBE/Hygro] vector) was purchased from Promega (Madison, WI, USA). Whole-mount in situ hybridisation was performed as described previously¹⁰¹. Fluorescence in situ hybridisation was performed as described previously¹⁰². Digoxigenin- or FITC-labelled RNA antisense probes were prepared from plasmids containing *n-cadherin*, *dbx1b*, *olig2*, *foxa2*, *cdx4*, *foxo3b*, *sesn3*, *lnx1*, *tcima*, *puma*, *wnt8a*, *shh*, *GFP*, *Emerald luciferase*, or *firefly luciferase*. Images were obtained using an FV3000 confocal laser scanning microscope.

Whole-mount multiplex in situ hybridisation chain reaction (HCR)

We followed the protocol suggested by Nepagene (Chiba, Japan), as described previously¹⁰³. The probes used were as follows: *foxo3b* and *dbx1b* (sequences of the probes are provided in Supplementary

Table 3). Images were obtained using an FV3000 confocal laser scanning microscope.

Reverse transcription polymerase chain reaction

For qPCR analysis, cDNA was synthesised using the ReverTra Ace qPCR RT master mix with genomic DNA remover (#FSQ-301; Toyobo, Osaka, Japan). qPCR analysis was conducted on a Stratagene Mx3000P qPCR system using THUNDERBIRD SYBR qPCR Mix (#QPS-201; Toyobo) using the following conditions: 95 °C (1 min), 45 cycles at 95 °C (15 s) and 60 °C (35 s). A standard curve was used to determine the relative mRNA abundance. The β -actin gene was used as a normalisation control. The primers used were as follows: 5'-taaggcaagcagagggtgttc-3' (*afg1lb* Fw1), 5'-ttctctgttcggttcctt-3' (*afg1lb* Rv1), 5'-ttgaatcaatcatggcg-3' (*afg1lb* Fw2), 5'-gtgtcgaacacctctgctt-3' (*afg1lb* Rv2), 5'-gagcaccctgacaagagac-3' (*foxo3b* Fw), 5'-gccggatggagttcttccaa-3' (*foxo3b* Rv), 5'-tggaacttgagcaggagatgggaa-3' (β -actin Fw), and 5'-aaggtgtctcatggataccgcaa-3' (β -actin Rv).

Histology

Dechorionated larvae were fixed in 4% paraformaldehyde overnight at 4 °C, solidified in iPGell (Genostaff, Tokyo, Japan), placed in 10 and 20% sucrose/PBS until the tissues were submerged, and in 30% sucrose/PBS overnight at 4 °C. iPGell-solidified larvae were embedded in a Tissue-Tek optimal cutting temperature (OCT) freezing medium (Sakura Finetek, Tokyo, Japan). Slices (20 μ m thick) were prepared using a Thermo Fisher Scientific HM525NX cryostat and stored at -80 °C until used (Fig. 2b, 4a; Supplementary Fig. 1a).

Gene set enrichment analysis (GSEA)

GSEA against RNA-seq data of β -catCA-mosaicly introduced (Mosaic) or ubiquitously β -catCA-expressing (Ubiquitous) zebrafish embryos (GEO accession code: GSE133526)⁷ was performed using RaNA-seq¹⁰⁴.

Mouse maintenance

Adult mice were maintained under a 12 h light/12 h dark cycle at 22 °C, 55% humidity. B6D2F1/Jcl (C57BL/6 N x DBA/2 N) F1 female mice were purchased from CLEA Japan, Inc. (Tokyo, Japan). Embryos were obtained from 3-week-old B6D2F1/Slc F1 female mice. Mice were maintained under specific pathogen-free conditions at the Animal Facility of the Frontier of Biosciences, Osaka University. The Animal Care and Use Committee of the Graduate School of Frontier Biosciences, Osaka University, approved all mice experiments (FBS Permit# FBS-20-001).

Mouse embryo culture and inhibitor treatment

Mouse embryos were obtained from the inter-crosses of B6D2F1/Jcl mice at the one- or two-cell stage using standard protocols¹⁰⁵ and were cultured in wells of a 72-well MiniTray (Nunc 136528) containing 10 μ L of Potassium Simplex optimised medium (KSOM; ARK resource, Kumamoto, Japan) covered with 5 μ L of mineral oil at 37 °C in a 5% CO₂ incubator. Embryos were cultured in KSOM containing 200 mM of Z-VAD-FMK (3118-v; Peptide Institute Inc., Osaka, Japan) and 0.4% DMSO from the early blastocyst stage to the late blastocyst stage to suppress apoptosis. Control embryos were cultured in KSOM containing 0.4% DMSO.

Immunofluorescent staining and image acquisition of mouse embryos

Immunofluorescence staining of embryos was performed using a 72-well MiniTray (Nunc 136528), as described previously¹¹, with slight modifications. Embryos were fixed in 4% paraformaldehyde in PBS for 5 min at 28.5 °C washed and permeabilised twice with 0.1% Triton X-100 in PBS (0.1% PBST) for 1 min at room temperature. The embryos were then blocked with 2% donkey serum in 0.1% PBST (blocking solution) and incubated overnight with primary antibodies in a blocking solution at

4 °C. After washing three times in 0.1% PBST for 1 min, the embryos were incubated with the secondary antibodies and Hoechst33342 (H342, 1/1000; Dojindo, Jawa Tengah, Indonesia) in 0.1% PBST for over 1 h at room temperature. After two washes in PBS, the embryos were placed in a PBS drop on a glass-based dish, and confocal images were obtained using a Nikon A1 inverted confocal microscope (Tokyo, Japan). Images were analysed using NIS-Elements AR analysis (Nikon) or IMARIS software (Bitplane, Belfast, UK). The following antibodies were used: mouse monoclonal anti-YAP1 antibody (H00010413-MO1, 1/100; Abnova, Taipei, Taiwan), rabbit monoclonal anti-FOXO3 (2497S, 1/100; Cell Signalling Technology), Alexa Fluor Plus 488-conjugated donkey anti-mouse antibody (A32766, 1/1000; Thermo Fisher Scientific), Alexa Fluor Plus 555-conjugated donkey anti-rabbit antibody (A32794, 1/1000; Invitrogen), and Alexa Fluor Plus 647-conjugated donkey anti-goat antibody (A21447, 1/1000; Invitrogen).

Analysis of *Foxo3* expression in post-implantation embryo loser cells

Single-cell RNA-seq data from E5.5 mouse embryos cultured for 16 h with or without a caspase inhibitor (accession number E-MTAB-80-640)¹² were re-analysed using Seurat 4.0.0¹⁰⁶. Six clusters, Epiblast_1 (Epi_1), Epiblast_2 (Epi_2), Epiblast_3 (Epi_3), Loser, Extra-embryonic ectoderm (ExE), and Visceral endoderm (VisEn), were identified based on the expression of marker genes.

Statistical analyses

Larvae without severe morphological defects were selected for imaging in each experiment. Differences between groups were examined using a two-tailed unpaired Student's *t*-test, one-way analysis of variance (ANOVA), chi-square test in Prism 8 (GraphPad Software, San Diego, CA, USA) or Excel (Microsoft, Redmond, WA, USA), and DESeq2 (version 1.10.1) (The R Project for Statistical Computing). *p* values < 0.05 were considered significant. The representative images and plots were reproduced in at least two (Figs. 1d–f, 2c–f, 4a, b, e, 5b, e, 6a, c, d, h, j, and 7a, c–f and Supplementary Figs. 1a–c, 2c–i, 3a–e, f, 4b–d, f, 6a, b, e–g, 7a, b, d, 8a–c, 10a, b, e, g–i, and 12c–g) or three or more (Figs. 1b, 2b, 3b–e, 4c, f, g, 5a, c, d, f, h, i, and 6b, f, g, i and Supplementary Figs. 1d–f, 2a, b, 3f, g, 4a, e, g, h, 5a, b, f, 6b, 7c, 8d, 9a–c, f–h, 10c, d, f and 11b, c) independent experiments.

Reporting summary

Further information on research design is available in the Nature Portfolio Reporting Summary linked to this article.

Data availability

All the data supporting this study are available within the article, supplementary information, and source data. The previously published datasets re-analyzed in this work can be accessed as GSE133526 and E-MTAB-80-640. Source data are provided with this paper.

References

- Wolpert, L. Positional information and the spatial pattern of cellular differentiation. *J. Theor. Biol.* **25**, 1–47 (1969).
- Davidson, E. H. Emerging properties of animal gene regulatory networks. *Nature* **468**, 911–920 (2010).
- Ju, Y. S. et al. Somatic mutations reveal asymmetric cellular dynamics in the early human embryo. *Nature* **543**, 714–718 (2017).
- Jónsson, H. et al. Multiple transmissions of de novo mutations in families. *Nat. Genet.* **50**, 1674–1680 (2018).
- Mashiko, D. et al. Chromosome segregation error during early cleavage in mouse pre-implantation embryo does not necessarily cause developmental failure after blastocyst stage. *Sci. Rep.* **10**, 854 (2020).
- Currie, C. E. et al. The first mitotic division of human embryos is highly error prone. *Nat. Commun.* **13**, 6755 (2022).

7. Akieda, Y. et al. Cell competition corrects noisy Wnt morphogen gradients to achieve robust patterning in the zebrafish embryo. *Nat. Commun.* **10**, 4710 (2019).
8. Morata, G. & Ripoll, P. Minutes: mutants of drosophila autonomously affecting cell division rate. *Dev. Biol.* **42**, 211–221 (1975).
9. Bowling, S., Lawlor, K. & Rodríguez, T. A. Cell competition: the winners and losers of fitness selection. *Development* **146**, dev167486 (2019).
10. Clavería, C., Giovinazzo, G., Sierra, R. & Torres, M. Myc-driven endogenous cell competition in the early mammalian embryo. *Nature* **500**, 39–44 (2013).
11. Hashimoto, M. & Sasaki, H. Epiblast formation by TEAD-YAP-dependent expression of pluripotency factors and competitive elimination of unspecified cells. *Dev. Cell* **50**, 139–154.e5 (2019).
12. Lima, A. et al. Cell competition acts as a purifying selection to eliminate cells with mitochondrial defects during early mouse development. *Nat. Metab.* **3**, 1091–1108 (2021).
13. Hogan, C. et al. Characterization of the interface between normal and transformed epithelial cells. *Nat. Cell Biol.* **11**, 460–467 (2009).
14. Kajita, M. et al. Interaction with surrounding normal epithelial cells influences signalling pathways and behaviour of Src-transformed cells. *J. Cell Sci.* **123**, 171–180 (2010).
15. Haraoka, Y., Akieda, Y., Nagai, Y., Mogi, C. & Ishitani, T. Zebrafish imaging reveals TP53 mutation switching oncogene-induced senescence from suppressor to driver in primary tumorigenesis. *Nat. Commun.* **13**, 1417 (2022).
16. Rhiner, C. et al. Flower forms an extracellular code that reveals the fitness of a cell to its neighbors in drosophila. *Dev. Cell* **18**, 985–998 (2010).
17. Merino, M. M. et al. Elimination of unfit cells maintains tissue health and prolongs lifespan. *Cell* **160**, 461–476 (2015).
18. Meyer, S. N. et al. An ancient defense system eliminates unfit cells from developing tissues during cell competition. *Science* **346**, 1258236 (2014).
19. Alpar, L., Bergantiños, C. & Johnston, L. A. Spatially restricted regulation of spätzle/toll signaling during cell competition. *Dev. Cell* **46**, 706–719.e5 (2018).
20. Nagata, R., Nakamura, M., Sanaki, Y. & Igaki, T. Cell competition is driven by autophagy. *Dev. Cell* **51**, 99–112.e4 (2019).
21. Katsukawa, M., Ohsawa, S., Zhang, L., Yan, Y. & Igaki, T. Serpin facilitates tumor-suppressive cell competition by blocking toll-mediated Yki activation in drosophila. *Curr. Biol.* **28**, 1756–1767.e6 (2018).
22. Novitch, B. G., Chen, A. I. & Jessell, T. M. Coordinate regulation of motor neuron subtype identity and pan-neuronal properties by the bHLH repressor Olig2. *Neuron* **31**, 773–789 (2001).
23. Pierani, A. et al. Control of interneuron fate in the developing spinal cord by the progenitor homeodomain protein Dbx1. *Neuron* **29**, 367–384 (2001).
24. Park, H.-C., Mehta, A., Richardson, J. S. & Appel, B. olig2 is required for zebrafish primary motor neuron and oligodendrocyte development. *Dev. Biol.* **248**, 356–368 (2002).
25. Gribble, S. L., Nikolaus, O. B. & Dorsky, R. I. Regulation and function of Dbx genes in the zebrafish spinal cord. *Dev. Dyn. Off. Publ. Am. Assoc. Anat.* **236**, 3472–3483 (2007).
26. Lek, M. et al. A homeodomain feedback circuit underlies step-function interpretation of a Shh morphogen gradient during ventral neural patterning. *Development* **137**, 4051–4060 (2010).
27. Devoto, S. H., Melançon, E., Eisen, J. S. & Westerfield, M. Identification of separate slow and fast muscle precursor cells in vivo, prior to somite formation. *Development* **122**, 3371–3380 (1996).
28. Stickney, H. L., Barresi, M. J. & Devoto, S. H. Somite development in zebrafish. *Dev. Dyn. Off. Publ. Am. Assoc. Anat.* **219**, 287–303 (2000).
29. Blagden, C. S., Currie, P. D., Ingham, P. W. & Hughes, S. M. Notochord induction of zebrafish slow muscle mediated by Sonic hedgehog. *Genes Dev.* **11**, 2163–2175 (1997).
30. Jessell, T. M. Neuronal specification in the spinal cord: inductive signals and transcriptional codes. *Nat. Rev. Genet.* **1**, 20–29 (2000).
31. Dessaud, E., McMahon, A. P. & Briscoe, J. Pattern formation in the vertebrate neural tube: a sonic hedgehog morphogen-regulated transcriptional network. *Development* **135**, 2489–2503 (2008).
32. Ueda, Y., Shimizu, Y., Shimizu, N., Ishitani, T. & Ohshima, T. Involvement of sonic hedgehog and notch signaling in regenerative neurogenesis in adult zebrafish optic tectum after stab injury. *J. Comp. Neurol.* **526**, 2360–2372 (2018).
33. Incardona, J. P., Gaffield, W., Kapur, R. P. & Roelink, H. The teratogenic *Veratrum* alkaloid cyclopamine inhibits Sonic hedgehog signal transduction. *Development* **125**, 3553–3562 (1998).
34. Tsai, T. Y.-C. et al. An adhesion code ensures robust pattern formation during tissue morphogenesis. *Science* **370**, 113–116 (2020).
35. Lele, Z. et al. *parachute / n-cadherin* is required for morphogenesis and maintained integrity of the zebrafish neural tube. *Development* **129**, 3281–3294 (2002).
36. Franklin, J. L. & Sargent, T. D. Ventral neural cadherin, a novel cadherin expressed in a subset of neural tissues in the zebrafish embryo. *Dev. Dyn.* **206**, 121–130 (1996).
37. Sun, Y., Tseng, W.-C., Fan, X., Ball, R. & Dougan, S. T. Extra-embryonic signals under the control of MGA, Max, and Smad4 are required for dorsoventral patterning. *Dev. Cell* **28**, 322–334 (2014).
38. Carter, M. E. & Brunet, A. FOXO transcription factors. *Curr. Biol.* **17**, R113–R114 (2007).
39. Xie, X., Liu, J.-X., Hu, B. & Xiao, W. Zebrafish foxo3b negatively regulates canonical Wnt signaling to affect early embryogenesis. *PLoS ONE* **6**, e24469 (2011).
40. Nogueira, V. et al. Akt determines replicative senescence and oxidative or oncogenic premature senescence and sensitizes cells to oxidative apoptosis. *Cancer Cell* **14**, 458–470 (2008).
41. Han, J. et al. Expression of *bbc3*, a pro-apoptotic BH3-only gene, is regulated by diverse cell death and survival signals. *Proc. Natl Acad. Sci. USA* **98**, 11318–11323 (2001).
42. Nakano, K. & Vousden, K. H. PUMA, a novel proapoptotic gene, is induced by p53. *Mol. Cell* **7**, 683–694 (2001).
43. Yu, J., Zhang, L., Hwang, P. M., Kinzler, K. W. & Vogelstein, B. PUMA induces the rapid apoptosis of colorectal cancer cells. *Mol. Cell* **7**, 673–682 (2001).
44. You, H. et al. FOXO3a-dependent regulation of Puma in response to cytokine/growth factor withdrawal. *J. Exp. Med.* **203**, 1657–1663 (2006).
45. You, H., Yamamoto, K. & Mak, T. W. Regulation of transactivation-independent proapoptotic activity of p53 by FOXO3a. *Proc. Natl Acad. Sci. USA* **103**, 9051–9056 (2006).
46. Tucka, J. et al. Akt1 regulates vascular smooth muscle cell apoptosis through FoxO3a and Apaf1 and protects against arterial remodeling and atherosclerosis. *Arterioscler. Thromb. Vasc. Biol.* **34**, 2421–2428 (2014).
47. Boldin, M. P., Goncharov, T. M., Goltseve, Y. V. & Wallach, D. Involvement of MACH, a novel MORT1/FADD-interacting protease, in Fas/APO-1- and TNF receptor-induced cell death. *Cell* **85**, 803–815 (1996).
48. Muzio, M. et al. FLICE, a novel FADD-Homologous ICE/CED-3-like protease, is recruited to the CD95 (Fas/APO-1) death-inducing signaling complex. *Cell* **85**, 817–827 (1996).
49. Alessi, D. R., Barry Caudwell, F., Andjelkovic, M., Hemmings, B. A. & Cohen, P. Molecular basis for the substrate specificity of protein kinase B; comparison with MAPKAP kinase-1 and p70 S6 kinase. *FEBS Lett.* **399**, 333–338 (1996).

50. Brunet, A. et al. Akt promotes cell survival by phosphorylating and inhibiting a forkhead transcription factor. *Cell* **96**, 857–868 (1999).
51. Lütznér, N., Kalbacher, H., Krones-Herzig, A. & Rösl, F. FOXO3 is a glucocorticoid receptor target and regulates LKB1 and its own expression based on cellular AMP levels via a positive auto-regulatory loop. *PLoS ONE* **7**, e42166 (2012).
52. Seoane, J., Le, H.-V., Shen, L., Anderson, S. A. & Massagué, J. Integration of Smad and Forkhead Pathways in the control of neuroepithelial and glioblastoma cell proliferation. *Cell* **117**, 211–223 (2004).
53. Joly, J.-S. et al. Expression of a zebrafish caudal homeobox gene correlates with the establishment of posterior cell lineages at gastrulation. *Differentiation* **50**, 75–87 (1992).
54. Sunagawa, G. A. et al. Mammalian reverse genetics without crossing reveals Nr3a as a short-sleeper gene. *Cell Rep.* **14**, 662–677 (2016).
55. Wu, R. S. et al. A rapid method for directed gene knockout for screening in G0 Zebrafish. *Dev. Cell* **46**, 112–125.e4 (2018).
56. Suzuki, H. et al. De novo non-synonymous CTR9 variants are associated with motor delay and macrocephaly: human genetic and zebrafish experimental evidence. *Hum. Mol. Genet.* **31**, 3846–3854 (2022).
57. Kon, S. et al. Cell competition with normal epithelial cells promotes apical extrusion of transformed cells through metabolic changes. *Nat. Cell Biol.* **19**, 530–541 (2017).
58. Sancho, M. et al. Competitive interactions eliminate unfit embryonic stem cells at the onset of differentiation. *Dev. Cell* **26**, 19–30 (2013).
59. Hu, B. et al. Zebrafish eaf1 suppresses foxo3b expression to modulate transcriptional activity of gata1 and spi1 in primitive hematopoiesis. *Dev. Biol.* **388**, 81–93 (2014).
60. Gao, L. et al. FOXO genes in channel catfish and their response after bacterial infection. *Dev. Comp. Immunol.* **97**, 38–44 (2019).
61. Villa del Campo, C., Claveria, C., Sierra, R. & Torres, M. Cell competition promotes phenotypically silent cardiomyocyte replacement in the mammalian heart. *Cell Rep.* **8**, 1741–1751 (2014).
62. Ellis, S. J. et al. Distinct modes of cell competition shape mammalian tissue morphogenesis. *Nature* **569**, 497–502 (2019).
63. Sun, X.-L. et al. Stem cell competition driven by the Axin2-p53 axis controls brain size during murine development. *Dev. Cell* **58**, 744–759.e11 (2023).
64. Adachi-Yamada, T., Fujimura-Kamada, K., Nishida, Y. & Matsumoto, K. Distortion of proximodistal information causes JNK-dependent apoptosis in *Drosophila* wing. *Nature* **400**, 166–169 (1999).
65. Adachi-Yamada, T. & O'Connor, M. B. Morphogenetic apoptosis: a mechanism for correcting discontinuities in morphogen gradients. *Dev. Biol.* **251**, 74–90 (2002).
66. Van Den Brink, G. R. et al. Indian Hedgehog is an antagonist of Wnt signaling in colonic epithelial cell differentiation. *Nat. Genet.* **36**, 277–282 (2004).
67. Farin, H. F. et al. Visualization of a short-range Wnt gradient in the intestinal stem-cell niche. *Nature* **530**, 340–343 (2016).
68. Wang, C. et al. Expansion of hedgehog disrupts mesenchymal identity and induces emphysema phenotype. *J. Clin. Investig.* **128**, 4343–4358 (2018).
69. Powell, D. R. et al. Cdon promotes neural crest migration by regulating N-cadherin localization. *Dev. Biol.* **407**, 289–299 (2015).
70. Van Der Vos, K. E. & Coffey, P. J. FOXO-binding partners: it takes two to tango. *Oncogene* **27**, 2289–2299 (2008).
71. Daitoku, H., Sakamaki, J. & Fukamizu, A. Regulation of FoxO transcription factors by acetylation and protein–protein interactions. *Biochim. Biophys. Acta BBA - Mol. Cell Res.* **1813**, 1954–1960 (2011).
72. Calissi, G., Lam, E. W.-F. & Link, W. Therapeutic strategies targeting FOXO transcription factors. *Nat. Rev. Drug Discov.* **20**, 21–38 (2021).
73. Hagenbuchner, J. & Ausserlechner, M. J. Mitochondria and FOXO3: breath or die. *Front. Physiol.* **4**, 147 (2013).
74. Kinzler, K. W. et al. Identification of FAP locus genes from chromosome 5q21. *Science* **253**, 661–665 (1991).
75. Nishishio, I. et al. Mutations of chromosome 5q21 genes in FAP and colorectal cancer patients. *Science* **253**, 665–669 (1991).
76. Oro, A. E. et al. Basal cell carcinomas in mice overexpressing sonic hedgehog. *Science* **276**, 817–821 (1997).
77. Xie, J. et al. Activating smoothened mutations in sporadic basal-cell carcinoma. *Nature* **391**, 90–92 (1998).
78. Fei, M. et al. Low expression of Foxo3a is associated with poor prognosis in ovarian cancer patients. *Cancer Investig.* **27**, 52–59 (2009).
79. Shou, Z., Lin, L., Liang, J., Li, J.-L. & Chen, H.-Y. Expression and prognosis of FOXO3a and HIF-1 α in nasopharyngeal carcinoma. *J. Cancer Res. Clin. Oncol.* **138**, 585–593 (2012).
80. Willcox, B. J. et al. FOXO3A genotype is strongly associated with human longevity. *Proc. Natl Acad. Sci. USA* **105**, 13987–13992 (2008).
81. Martins, R., Lithgow, G. J. & Link, W. Long live FOXO: unraveling the role of FOXO proteins in aging and longevity. *Aging Cell* **15**, 196–207 (2016).
82. Timmers, P. R. H. J., Wilson, J. F., Joshi, P. K. & Deelen, J. Multi-variate genomic scan implicates novel loci and haem metabolism in human ageing. *Nat. Commun.* **11**, 3570 (2020).
83. Zhang, W. et al. A single-cell transcriptomic landscape of primate arterial aging. *Nat. Commun.* **11**, 2202 (2020).
84. Liu, X. et al. Forkhead Transcription Factor 3a (FOXO3a) Modulates Hypoxia Signaling via Up-regulation of the von Hippel-Lindau Gene (VHL). *J. Biol. Chem.* **291**, 25692–25705 (2016).
85. Wada, H. et al. Wnt/Dkk negative feedback regulates sensory organ size in Zebrafish. *Curr. Biol.* **23**, 1559–1565 (2013).
86. Sasaki, H., Hui, C., Nakafuku, M. & Kondoh, H. A binding site for Gli proteins is essential for *HNF-3* floor plate enhancer activity in transgenics and can respond to Shh in vitro. *Development* **124**, 1313–1322 (1997).
87. Shimizu, N., Kawakami, K. & Ishitani, T. Visualization and exploration of Tcf/Lef function using a highly responsive Wnt/ β -catenin signaling-reporter transgenic zebrafish. *Dev. Biol.* **370**, 71–85 (2012).
88. Taipale, J. et al. Effects of oncogenic mutations in smoothened and patched can be reversed by cyclopamine. *Nature* **406**, 1005–1009 (2000).
89. Kinzler, K. W., Ruppert, J. M., Bigner, S. H. & Vogelstein, B. The GLI gene is a member of the Kruppel family of zinc finger proteins. *Nature* **332**, 371–374 (1988).
90. Zhang, Y. et al. Structural basis for cholesterol transport-like activity of the hedgehog receptor patched. *Cell* **175**, 1352–1364.e14 (2018).
91. Jia, S., Ren, Z., Li, X., Zheng, Y. & Meng, A. smad2 and smad3 are required for mesendoderm induction by transforming growth factor-beta/nodal signals in zebrafish. *J. Biol. Chem.* **283**, 2418–2426 (2008).
92. Wang, F. et al. Structures of KIX domain of CBP in complex with two FOXO3a transactivation domains reveal promiscuity and plasticity in coactivator recruitment. *Proc. Natl Acad. Sci. USA* **109**, 6078–6083 (2012).
93. Zhang, J. et al. Visualization of caspase-3-like activity in cells using a genetically encoded fluorescent biosensor activated by protein cleavage. *Nat. Commun.* **4**, 2157 (2013).
94. Bindels, D. S. et al. mScarlet: a bright monomeric red fluorescent protein for cellular imaging. *Nat. Methods* **14**, 53–56 (2017).
95. Yamamoto, K., Ichijo, H. & Korsmeyer, S. J. BCL-2 Is Phosphorylated and Inactivated by an ASK1/Jun N-Terminal protein kinase pathway normally activated at G₂/M. *Mol. Cell. Biol.* **19**, 8469–8478 (1999).

96. Ansai, S. et al. Genome editing reveals fitness effects of a gene for sexual dichromatism in Sulawesian fishes. *Nat. Commun.* **12**, 1350 (2021).
97. Hwang, W. Y. et al. Efficient genome editing in zebrafish using a CRISPR-Cas system. *Nat. Biotechnol.* **31**, 227–229 (2013).
98. Kimura, Y., Hisano, Y., Kawahara, A. & Higashijima, S. Efficient generation of knock-in transgenic zebrafish carrying reporter/driver genes by CRISPR/Cas9-mediated genome engineering. *Sci. Rep.* **4**, 6545 (2014).
99. Kardash, E. Current Methods in Zebrafish Research. *Mater. Methods* **2**, 109 (2012).
100. Lee, Y. A., Cho, E. J. & Yokozawa, T. Protective Effect of Persimmon (Diospyros kaki) Peel Proanthocyanidin against Oxidative Damage under H₂O₂-Induced Cellular Senescence. *Biol. Pharm. Bull.* **31**, 1265–1269 (2008).
101. Thisse, C. & Thisse, B. High-resolution in situ hybridization to whole-mount zebrafish embryos. *Nat. Protoc.* **3**, 59–69 (2008).
102. Brend, T. & Holley, S. A. Zebrafish whole mount high-resolution double fluorescent in situ hybridization. *J. Vis. Exp. JoVE* 1229 <https://doi.org/10.3791/1229>. (2009)
103. Tsuneoka, Y. & Funato, H. Modified in situ Hybridization Chain Reaction Using Short Hairpin DNAs. *Front. Mol. Neurosci.* **13**, 75 (2020).
104. Prieto, C. & Barrios, D. RaNA-Seq: interactive RNA-Seq analysis from FASTQ files to functional analysis. *Bioinformatics* **36**, 1955–1956 (2020).
105. Behringer, R. *Manipulating the Mouse Embryo: A Laboratory Manual*. (Cold Spring Harbor Laboratory Press, 2014).
106. Hao, Y. et al. Integrated analysis of multimodal single-cell data. *Cell* **184**, 3573–3587.e29 (2021).

Acknowledgements

We thank K. Kawakami, P. Beachy, S. Ishii, B. Vogelstein, B. Li, D. Gadella, and S. Korsmeyer for providing plasmids, and D. Masui and Ishitani lab members for their helpful discussions, technical support, and fish maintenance. This research was supported by the Takeda Science Foundation (T.I.), SECOM Science and Technology Foundation (T.I.), KOSE Cosmetology Foundation (T.I.), Astellas Foundation for Research on Metabolic Disorders (2022A1209) (Y.A.), JST SPRING (K.M.), JSPS Fellows (24KJ16170) (K.M.), Grant-in-Aid for Transformative Research Areas(A) (21H05287) (T.I.) (21H05288) (H.S.), Scientific Research (B) (22H02820) (T.I.), Challenging Exploratory Research (23K18242) (T.I.), Scientific Research on Innovative Areas (22H04845) (Y.A.), and Early-Career Scientists (21K15085) (Y.A.), MEXT Promotion of Development of a Joint Usage/Research System Project: Coalition of Universities for Research Excellence (CURE) Program (JPMXP1323015484) (T.I.), and AMED-CREST (24gm2010001h0001) (T.I.).

Author contributions

Conception and design: K.M., Y.A., T.I. wrote the main manuscript text; K.M., Y.A., T.I. analysed the data; K.M., Y.A., Y.H., N.H., H.S., T.I. prepared the figures. All authors have reviewed the manuscript.

Competing interests

The authors declare no competing interests.

Additional information

Supplementary information The online version contains supplementary material available at <https://doi.org/10.1038/s41467-024-55108-x>.

Correspondence and requests for materials should be addressed to Tohru Ishitani.

Peer review information *Nature Communications* thanks Jungmin Choi, Miguel Torres and the other, anonymous, reviewer(s) for their contribution to the peer review of this work. A peer review file is available.

Reprints and permissions information is available at <http://www.nature.com/reprints>

Publisher's note Springer Nature remains neutral with regard to jurisdictional claims in published maps and institutional affiliations.

Open Access This article is licensed under a Creative Commons Attribution-NonCommercial-NoDerivatives 4.0 International License, which permits any non-commercial use, sharing, distribution and reproduction in any medium or format, as long as you give appropriate credit to the original author(s) and the source, provide a link to the Creative Commons licence, and indicate if you modified the licensed material. You do not have permission under this licence to share adapted material derived from this article or parts of it. The images or other third party material in this article are included in the article's Creative Commons licence, unless indicated otherwise in a credit line to the material. If material is not included in the article's Creative Commons licence and your intended use is not permitted by statutory regulation or exceeds the permitted use, you will need to obtain permission directly from the copyright holder. To view a copy of this licence, visit <http://creativecommons.org/licenses/by-nc-nd/4.0/>.

© The Author(s) 2024